5-2021

Application of Flow and Ion Data to Estimate Ungaged Inflows and Losses in Urban and Agricultural Sub-Reaches of the Logan River Observatory

Hyrum Tennant
Utah State University

APPLICATION OF FLOW AND ION DATA TO ESTIMATE UNGAGED INFLOWS AND LOSSES IN URBAN AND AGRICULTURAL SUB-REACHES OF THE LOGAN RIVER OBSERVATORY

by

Hyrum Tennant

A thesis submitted in partial fulfillment
of the requirements for the degree

of

MASTER OF SCIENCE

in

Civil and Environmental Engineering

Approved:

Bethany T. Neilson, Ph.D. Major Professor	Mathew P. Miller, Ph.D. Committee Member
Tiangfang Xu, Ph.D. Committee Member	D. Richard Culter, Ph.D. Interim Vice Provost of Graduate Studies

UTAH STATE UNIVERSITY
Logan, Utah

2021

ABSTRACT

Application of Flow and Ion Data to Estimate Ungaged Inflows and Losses in Urban and Agricultural Sub-Reaches of the Logan River Observatory

by

Hyrum Tennant, Master of Science

Utah State University, 2021

Major Professor: Dr. Bethany T. Neilson
Department: Civil and Environmental Engineering

Streams in semi-arid urban and agricultural environments are often heavily diverted for anthropogenic purposes. However, they simultaneously receive substantial inflows from a variety of ungaged sources including stormwater returns, tile drainage, and irrigation runoff that help sustain flow during dry periods. Due to the inability to identify sources or directly gage many of these inflows, there is a clear need for methods to understand source origination while quantifying potential gains and losses over highly impacted reaches. In the context of the Logan River Observatory, historical gage data illustrate the importance of ungaged and unidentified inflows on maintaining or enhancing flows in both urban and agricultural reaches containing large diversions. To understand the various inflows in this portion of the Logan River, we first analyzed water samples for ions collected from a subset of representative inflow sources, then applied clustering analyses to establish inflow source classifications and associated ion concentration ranges. These representative concentration ranges, combined with mainstem flow and river ion samples taken at sub-reach scales, allow for the application

of flow and mass balances to quantify inflow rates from different sources as well as any losses. These calculations demonstrate significant gains and losses occurring in many sub-reaches during three sampling events. The dominant land use (urban or agriculture) and flow regime at the time of sampling were the primary drivers of exchanges. These exchanges were most important below large diversions during low flow conditions. This highlights the need to classify inflow sources (urban or agriculture, surface or groundwater) and estimate their contributions to anticipate instream consequences of land use and water management decisions. As irrigation and water conveyance practices become more efficient, a portion of these ungaged inflows could be diminished or eliminated, thus further depleting streamflow during dry periods.

(72 pages)

PUBLIC ABSTRACT

Application of Flow and Ion Data to Estimate Ungaged Inflows and Losses in Urban and Agricultural Sub-Reaches of the Logan River Observatory

Hyrum Tennant

Streams in urban and agricultural environments are often heavily diverted for irrigation and drinking water purposes. These streams can receive inflow from unmeasured sources including stormwater returns, groundwater drains, and irrigation runoff that will help sustain flow during dry periods. Due to an inability to identify the source of most of these inflows or directly measure their volumes, there is a clear need for identification and quantification methods. Streamflow data from the Logan River Observatory illustrates the importance of unidentified inflows in sections influenced by large diversions. To understand the role of unidentified inflows and possible outflows in this portion of the Logan River, we first collected ion samples from a subset of representative inflow sources and then applied clustering analyses to establish a categorization scheme. Representative concentration ranges for each category of inflow sources, combined with ion samples and streamflow measurements of the Logan River were used in a system of equations to calculate both inflow and loss volumes. The calculated inflows and losses were observed to be most influential at maintaining flow downstream of large diversions and at times of low streamflow in the summer and fall. This highlights the need to better understand and quantify inflow sources. As management practices become more efficient, without an understanding inflow sources

and contributions, a portion of these inflows could unknowingly be diminished or eliminated and no longer sustain stream flows during dry periods.

ACKNOWLEDGMENTS

I would like to thank Dr. Bethany Neilson for her guidance and patience with me both as an undergraduate researcher and the last few years as a master's candidate. Thanks to Dr. Matthew Miller and Dr. Tianfang Xu for serving on my committee and their guidance in developing this project.

I would like to thank all the members of the Neilson lab group including, Bryce Mihalevich, Eillen Lukens, Dane Brophy, Abbygael Johnson, Scott Mershon, Makail Lunt, Nikki Quinney, Bryce Mihalevich, Dr. Caleb Buahin, Dr. Milada Majerova, Mitchell Rasmussen, Rezaul Haider, and Leah Richardson. A special thanks to Dr. Noah Schmadel, and Dr. Tyler King for showing me what it is to be a researcher. Thanks to Michelle Barnes and Trinity Stout for their mentorship and help in the field, advice, ideas, and conversation that resulted in this project. Thanks to Patrick Strong for his constant ideas, conversation, and field help. Additional thanks to Rachel Gabor, Malory Millington, Andrew Gelderloos, Paul Brooks, Michelle Baker, and Dave Epstein for their help with synoptic sampling and field efforts.

I would like to recognize the funding sources that made this research possible, the Utah Water Research Laboratory, USU Vice President of Research Office, USU College of Natural Resources, USU College of Engineering, USU Ecology Center, the USGS, the Utah State Legislature through the Utah Division of Water Resources, Logan City, Cache Water District, and the NSF EPSCoR grant IIA 1208732 awarded to Utah State University as part of the State of Utah Research Infrastructure Improvement Award.

Finally, a special thanks to my parents for the love, support, and instilling in me the values of hard work, education, and a love for the outdoors.

CONTENTS

Page

LIST OF TABLES

LIST OF FIGURES

CHAPTER I
INTRODUCTION

In natural systems, rivers and streams gain and lose water over variable scales (Covino, McGlynn, & Mallard, 2011; Schmadel, Neilson, & Kasahara, 2014). These gains and losses, or hydrologic exchanges, determine longitudinal variability of streamflow in natural systems. Inflows can include groundwater discharge and runoff from precipitation events and snowmelt. Outflows can be due to losses to groundwater or evapotranspiration. Long hyporheic exchange flow paths could result in a gain or a loss. Surface water inflows have shorter travel times compared to groundwater and are often related to precipitation events (e.g., overland flow). Groundwater inflows typically have longer flow path lengths and residence times (Tesoriero, Duff, Saad, Spahr, & Wolock, 2013; Van Meter & Basu, 2015) while providing a stable source of base flow (Winter, 1995). Outflow to groundwater can be highly variable due to local head gradients and geology (Winter, Harvey, Franke, & Alley, 1998), but is often a primary source of streamflow loss.

In urban and agricultural systems, mechanisms of streamflow gains and losses are similar to those in natural systems, but include other sources and sinks due to anthropogenic activities. Anthropogenic streamflow losses are primarily due to diversions for urban and agricultural irrigation where water is distributed across the landscape via canals, ditches or pipes. These diversions commonly put additional stress on streams during low flows (Scanlon, Jolly, Sophocleous, & Zhang, 2007) and increase the risk of downstream reaches running dry (Wang & Cai, 2009). Anthropogenic inflows include point sources such as storm drain outlets, French drains, tile drain systems, wastewater returns, return flow from diversions, and non-point sources such as agricultural and urban irrigation runoff. During

base flow conditions, or times when streamflow is dominantly made up of natural groundwater discharge, anthropogenic inflows from high density urban and agricultural areas can contribute a significant fraction of total streamflow and offset the influence of large diversions (Bhaskar & Welty, 2012; Claessens, Hopkinson, Rastetter, & Vallino, 2006; Garcia-Fresca, 2007). However, increases in withdrawals or management actions focused on improved efficiency (e.g., stormwater handling, conveyance, or irrigation) could have unanticipated consequences and further reduce streamflow in dewatered reaches.

To understand the resilience of streams and rivers to maintain instream flow in urban and agricultural areas influenced by withdrawals, there is a need to estimate inflow and outflow rates and identify their sources (Bhaskar & Welty, 2001). While large surface inflows and diversions are easily and often gaged for management purposes, inflows from other sources such as irrigation runoff and storm drain outlets, as well as most outflows, are difficult to directly measure. Different approaches have been applied to estimate reach scale gains and losses. The simplest method is based on differencing flow from two different locations to get net gains or losses (McCallum, Cook, Berhane, Rumpf, & McMahon, 2012; Schmadel et al., 2014). Many have combined flow and solute mass balances to estimate gross inflows and outflows (Cook, 2013; McCallum et al., 2012; Neilson et al., 2018). However, when applying methods to estimate gains and losses, a series of assumptions are required and some estimate of individual inflow source or end member concentrations are required.

In anthropogenically influenced watersheds, inflow sources can be diverse and difficult to identify. It is common that any one inflow is the product of multiple sources, leaving end member sources and concentrations unknown (Gburek & Folmar, 1999; Ryan, Welty, & Larson, 2010). However, methods that can broadly classify inflow sources (e.g., agricultural surface water or agricultural groundwater) based on reasonable amounts of chemical sampling could provide the needed information to estimate gross inflows and outflows. Towards this end, we develop a classification scheme using different quantities of inflow ion samples to identify relevant ion concentration ranges. When combined with a detailed seepage study and river ion samples, a system of flow and mass balance equations can be used to estimate the outflow and surface and groundwater inflows from different sources at sub-reach scales. In the context of a case study in the urban and agricultural section of the Logan River, we illustrate how these estimates can provide management insights regarding sources that are maintaining instream flows to ensure beneficial uses are met.

CHAPTER II

METHODS

2.1 Study Area

The Logan River watershed (41.739034º, -111.795742º) is home to the Logan River Observatory (LRO), which operates a diverse set of aquatic and terrestrial monitoring sites that span the mountainous and valley portions of the watershed (see https://uwrl.usu.edu/lro/locations for a detailed map and access to data). The headwaters of the Logan River are located in Northern Utah and Southern Idaho (Figure 1a) with the course of the river flowing through the karst limestone geology of the Bear River Range (Spangler, 2001). The valley portion of the watershed is primarily composed of Lake Bonneville sediments with a clay layer abutting the river in many sections (Dover, 1995). Average annual precipitation in the watershed ranges from 44 cm (National Climate Data Center, NESDIS, NOAA, 2010) in the valley to 123 cm (USDA Natural Resources Conservation Service, 2020) in the canyon. The hydrology is dominated by snowmelt processes with peak flows occurring in late spring followed by sustained base flow through the late summer, fall, and winter. The average flow at the U.S. Geological Survey (USGS) gage 10109000 is 6.5 m^3/s (cms) which is located at the transition from the mountainous portion of the watershed to the valley (U.S. Geological Survey, 2020).

This study focuses on a 12-kilometer reach of the Logan River that spans the urban and agricultural areas in the valley portion of the watershed (Figure 1b). The LRO operates three mainstem gages, UWRL, Main Street, and Mendon Road, within this area (Figure 1b). Three major tributaries, the Blacksmith Fork River, Spring Creek, and Little

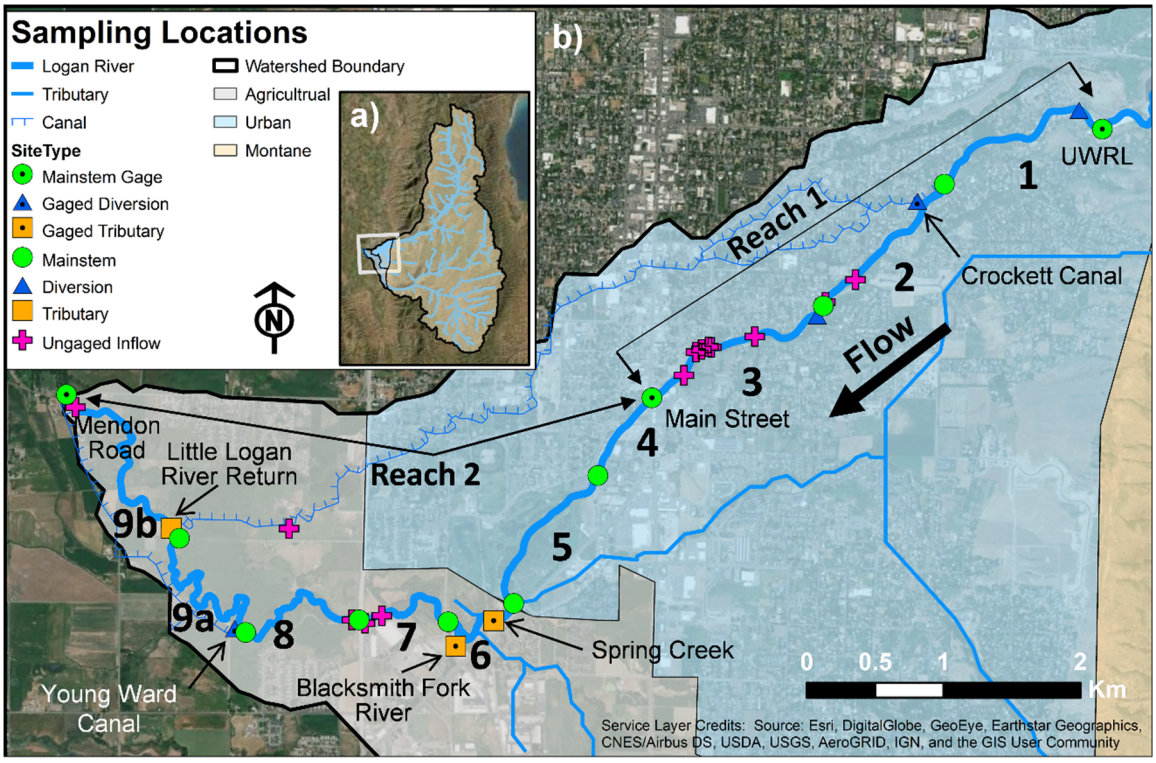

Figure 1. a) Logan River Watershed. b) Study area of the Logan River Watershed with the urban (blue) and agricultural (grey) areas highlighted and significant tributaries and canals shown. Sampling locations (mainstem, diversions, tributaries, and ungaged inflows) and sub-reaches 1 - 9b delineated by the mainstem sampling locations and gages.

Logan River Return, and two major diversions, the Crockett Canal and the Young Ward Canal, significantly influence the instream flows within the study reach (Figure 1b). Both the Blacksmith Fork and Spring Creek are gaged at their confluence with the Logan River by the LRO. These tributaries have mountain headwaters, but are heavily diverted for agricultural use during the growing season (May to October). Depending on the time of year springs, agricultural runoff, and urban runoff all contribute to the flow of these tributaries as they progress through their respective urban and agricultural areas.

The Crockett Canal is located at the upstream end of the urban area near the canyon mouth and supplies flow to the Little Logan River Return and several other canals that distribute water to urban irrigation systems and agricultural lands throughout the

valley. This diversion is only active during the growing season (May to October) with a mean flow of 1.8 cms (Utah Division of Water Rights, 2021a). Even though the Little Logan River Return is sourced primarily from the Crockett Canal diversion, it contributes water to the river year-round due to contributions from springs that flow into the canal over its course. The Young Ward Canal diverts water from the Logan River for agricultural irrigation during the growing season with a mean flow of 0.8 cms (Utah Division of Water Rights, 2021b). During low flows, this diversion often removes all the water in the river, leaving a dry channel downstream. Both the Crockett Canal and Young Ward Canal are gaged by the Utah Division of Water Rights (DWRi) at their respective points of diversion. To provide context regarding the magnitude of these diversions, the Logan River has an average flow of 16.7 cms in May and June and 4.3 cms in August and September at the USGS gage 10109000.

Within the agricultural areas, water is conveyed via canal networks (Figure A1). This diverted water is primarily used for flood irrigation of crops although some sprinkler irrigation does occur. Most water shares or rights are accessed using the canal system although some rights are fulfilled by diverting water directly from the river or through use of shallow wells adjacent to the river (Utah Division of Water Rights, 2020). There are a number of springs in the agricultural section, most of which flow into the canal network (Figure A1).

Within the urbanized portion of the watershed, diverted water is distributed across the landscape via a network of gutters and canals to meet urban irrigation demands. Any excess water left in the system after irrigation is returned to the river via ditches and storm drain outlets. Much of this urban irrigation water is applied via flood irrigation to

lawns and yards. Canal water is distributed within neighborhoods via head gates integrated into the curb-and-gutter system (Figure A1). Most residential parcels adjoining the river have water rights and small irrigation ditches that convey water the length of the parcel where excess water flows back into the river. There are a few springs within the urban area that are captured and diverted into the irrigation network (Figure A1). Additionally, in the urban area, French drains are used to lower the high-water table near the river. These drains can discharge directly to the river, but are also connected to the curb-and-gutter system and act as storm drain outlets during precipitation events (Figure A1).

It is necessary for a distinction to be made between inflows occurring in the urban areas and those occurring in agricultural areas. Combined, return inflows from the different anthropogenic activities within the watershed, along with underlying natural groundwater inflow, create a complex network of both point and distributed ungaged inflows. A subset of these inflow locations and some sources of these inflows were identified (Figure 1b). In an effort to classify different sources of inflows, the study area was divided into an urban and agricultural portion at Sub-reach 5 (Figure 1b). This division generally reflects the change in land cover and ungaged inflow sources (from piped urban inflows to more distributed agricultural inflows).

2.2 Data Collection

Streamflow data were reported at 15-minute intervals by gages operated by the LRO and DWRi. Details regarding LRO flow gaging station equipment, data telemetry, quality control procedures, and data dissemination are provided within Jones et al. (2017)

where they describe the initial installation of statewide infrastructure in the context of original National Science Foundation funded iUTAH - innovative Urban Transitions and Aridregion Hydro-sustainability project (http://iutahepscor.org). All raw and quality-controlled flow data are available at http://lrodata.usu.edu by selecting the "Site Code" of interest. For each site, rating curves are also available by selecting "Explore Rating Curve." A complete list of the gages and collected parameters in the Logan River Watershed including those operated/reported by the LRO, state, and federal agencies is provided in Table S1.

Daily mean streamflow was calculated from the 15-minute data at LRO and DWRi sites for use in the analysis presented here. The LRO mainstem gages were used to delineate two longer reaches, Reach 1, and Reach 2 (Figure 1b).

Three synoptic sampling efforts were conducted in June 2015, August 2015, and September 2019 to estimate the contributions from different ungaged inflows and outflows. A total of 39 samples were collected from the river and major tributaries and 22 samples from point sources of ungaged inflow across all sampling events. During each sampling event, discharge measurements were made along the mainstem of the Logan River which were used to divide the study reach into 9 sub-reaches (Figure 1b). An additional site was added during the September 2019 sampling event to better bracket the Little Logan River Return; this divided sub-reach 9 into Sub-reaches 9a and 9b. The flow in each of the identified major tributaries and diversions was also measured. A YSI SonTek Flowtracker Handheld Acoustic Doppler Velocimeter was used to make flow measurements using the velocity area method (Rantz, 1982). At the location of each discharge measurement, grab samples were collected from the thalweg and far enough

downstream of known inflows to allow for mixing. Samples were analyzed for anions (chloride, sulfate, nitrate) and cations (sodium, calcium, magnesium). Samples were filtered with a 0.45 um nylon filter into acid-washed LDPE bottles. Anion samples were frozen and cation samples were acidified with nitric acid and refrigerated. Samples were analyzed by ion chromatography using a Dionex DX-1300 ion chromatograph. Specific conductance was also measured in conjunction with collection of grab samples using a YSI 6920 V2 Sonde or a YSI EXO V1 Sonde. Grab samples were also collected from identified ungaged inflows (Figure 1b) that included a variety of urban storm drain outlets, French drains, agricultural irrigation return flows, and springs.

2.3 Hierarchical Clustering Analysis

The ion sample data collected from inflows for each of the three sampling events were investigated by sampling event and as a pooled composite dataset using an agglomerative Hierarchical Clustering Analysis (HCA) (Hastie, Tibshirani, & Friedman, 2009). HCA creates clusters of samples based on the dissimilarity of the ion concentration magnitudes via Ward's linkage method that uses an analysis of variance to identify clusters and the Euclidian distance to measure the similarity between samples (Liu et al., 2020; Moya, Raiber, Taulis, & Cox, 2015; Ward, 1963). By combining all data, it would be possible to determine if samples could be categorized consistently with local knowledge of the system and if composite HCA results similarly clustered samples into different source categories when compared to the results from individual events. It would also provide insight into ion concentration ranges for these broad categories and if significant changes in source occur during sampling events.

HCA analyses produce a dendrogram that was used to graphically represent the hierarchy of clusters resulting from cutting a dendrogram at different linkage values. Based on local knowledge of likely sources, and in some cases the presence of a sample(s) that could be visually traced to a known inflow source, the clusters were assigned a category of surface water or groundwater at a linkage distance of 250. At a linkage distance of 201, these categories could be further split based on the general location within the urban or agricultural portion of the watershed. In the end, four categories were established that included urban surface water, urban groundwater, agricultural surface water, and agricultural groundwater.

For each category, concentration ranges were calculated from composite dataset samples associated with the category and were assumed to fully represent inflows in that category. This process was repeated for each individual sampling event to similarly produce event-specific sets of concentration ranges that represented the inflows at the time of the sampling event. At the end of this process, we had a composite set of concentration ranges that could be applied across all flow regimes and event specific concentration ranges only valid for the flow conditions present during each sampling event. These ranges were used in subsequent calculations to compare and contrast the category assignments of different inflows, determine the influence of concentration ranges on sub-reach scale inflow estimates, and establish how different amounts of data influence interpretation and confidence in results.

2.4 Flow and Mass Balances

To determine the gains and losses within each reach or sub-reach (Figure 1) along the Logan River, a combination of flow and mass balance equations can be applied. First, a flow balance equation representative of each reach and sub-reach was written:

$$Q_2 - Q_{trib} + Q_{div} - Q_1 = \Delta Q, \quad (1)$$

where Q_1 is the discharge at the upstream end of the reach or sub-reach, Q_2 is the discharge at the downstream end of the reach or sub-reach, Q_{trib} is the discharge of any tributaries within the reach or sub-reach, Q_{div} is the discharge of any diversions removing water from the reach or sub-reach, and ΔQ is the net ungaged change in discharge within the reach or sub-reach. This equation provides estimates of net ungaged changes in discharge for Reaches 1 and 2 between LRO gaging stations over time.

To account for both gains and losses, the ΔQ term can be further expanded to represent ungaged inflow from both surface water and groundwater and outflow occurring within each sub-reach:

$$\Delta Q = Q_{sw} + Q_{gw} - Q_{out}, \quad (2)$$

where Q_{sw} is the sum of all ungaged surface water inflows within the sub-reach, Q_{gw} is the sum of all ungaged groundwater inflows in the sub-reach, and Q_{out} is the ungaged outflow within the sub-reach.

Substituting for ΔQ in Eqn. (1) yields:

$$Q_2 - Q_{trib} + Q_{div} - Q_1 = Q_{sw} + Q_{gw} - Q_{out}, \quad (3)$$

A similar solute mass balance equation can also be written for each sub-reach:

$$Q_2C_2 - Q_{trib}C_{trib} + Q_{div}C_{div} - Q_1C_1 = Q_{sw}C_{sw} + Q_{gw}C_{gw} - Q_{out}C_{out}, \quad (4)$$

where *C* is the concentration of a given ion associated with the corresponding flow (*Q)* value as indicated by the subscript.

Mathematically the inflows and outflow are lumped and represented as occurring at one point, respectively. The flow value of the outflow, Q_{out}, can be minimized by assuming the outflow occurs prior to the inflows (OI) or maximized by assuming the outflow occurs subsequent to all inflows (IO) (Payn et al., 2009; Peterson et al., 2010). The OI condition is represented by setting C_{out} to C_1 and the IO condition is represented by setting C_{out} to C_2. The mass balance equation was evaluated for both the OI and IO conditions allowing for the maximum and minimum possible values of the exchanges to be estimated. The resulting equation is:

$$Q_2C_2 - Q_{trib}C_{trib} + Q_{div}C_{div} - Q_1C_1 = Q_{sw}C_{sw} + Q_{gw}C_{gw} - Q_{out}C_{(1,2)}. \quad (5)$$

Values for C_{sw} and C_{gw} can then be set to the respective concentration ranges determined for the surface water and groundwater categories from the HCA for a given ion.

If we write an additional mass balance equation, but utilize the concentration ranges for an additional ion represented by the variable *B*, a solvable system of equations is established:

$$Q_2 - Q_{trib} + Q_{div} - Q_1 = Q_{sw} + Q_{gw} - Q_{out}, \quad (6)$$

$$Q_2C_2 - Q_{trib}C_{trib} + Q_{div}C_{div} - Q_1C_1 = Q_{sw}C_{sw} + Q_{gw}C_{gw} - Q_{out}C_{(1,2)}, \quad (7)$$

$$Q_2B_2 - Q_{trib}B_{trib} + Q_{div}B_{div} - Q_1B_1 = Q_{sw}B_{sw} + Q_{gw}B_{gw} - Q_{out}B_{(1,2)}. \quad (8)$$

This leaves us with three equations (Equations 6-8) with three unknowns (Q_{gw}, Q_{out}, Q_{sw}).

This system of equations was evaluated for all possible ion pairs represented by *B* and *C* and their associated concentration ranges from the HCA for each sub-reach

assuming IO and OI. A total of 1,000 random samples of $[C_{sw}, C_{gw}]$ were generated, assuming that each ion concentration is independent and follows a uniform distribution bounded by the concentration ranges of the surface water and groundwater categories identified by the HCA. Equations (6-8) were then solved for each of the 1,000 samples for each ion pair and for the IO and OI assumptions, respectively. Only when positive values were calculated for Q_{gw}, Q_{sw}, or Q_{out} (out of a possible 2000 total solutions per ion pair) were the results retained as part of the solution set. The solution sets for each ion pair were combined to create a solution set representing the range of possible values for Q_{gw}, Q_{sw}, and Q_{out}. For a better understanding of contributions, each solution for Q_{gw}, Q_{sw}, and Q_{out} was converted to relative percentages of the flow at the upstream end of the sub-reach:

$$\%Q_x = \frac{Q_x}{Q_1} \times 100\%, \tag{9}$$

where Q_x can equal Q_{gw}, Q_{sw}, or Q_{out}. Because the concentration ranges included all sources within a category, it is possible that only a small portion of the concentration range was representative of sources within a sub-reach. Additionally, it was possible that the established range did not represent the sources within a sub-reach. In both cases, it is plausible to obtain only a few feasible solutions from the 2000 possible solutions. In an effort to focus on only presenting robust estimates for the possible ranges of Q_{gw}, Q_{sw} and Q_{out}, we arbitrarily determined solution sets to be viable only if >100 solutions (or 5% of the 2000 total possible solutions) for different ion pairs were found. If there were less than 100 solutions, the results for the particular sub-reach were discarded,

assuming there was not enough information to represent this sub-reach or its inflow sources well.

Given many lines of evidence and the range of potential uncertainty due to the broad categorization, we again attempted to isolate results that were robust by only considering the inflow(s) or outflow within a sub-reach to be significant if the 1st-quartile of the range of viable solutions for the percent values of Q_{gw}, Q_{sw}, and Q_{out} had a magnitude greater than 5%. This limit was again arbitrarily set to ensure that only inflows with ranges greater than zero were being considered as having a notable effect on streamflow in our analysis.

This process was completed for both the urban and agricultural portions of the study reach using the HCA source category concentration ranges derived from the composite ion dataset to estimate ungaged groundwater and surface water inflows in each sub-reach. Similarly, the process was repeated with the three event-specific source category concentration ranges. Temporal and spatial trends in inflows and outflow were compared across the composite and three event-specific set of results to identify any patterns in the inflows and outflow occurring within the sub-reaches.

CHAPTER III

RESULTS

3.1 Flow and Ion Trends

Comparison of the LRO mainstem gages' (UWRL, Main Street, and Mendon Road, Figure 1b) hydrographs during water years 2015 and 2019 illustrate the increases in flow between the UWRL and Mendon Road gages during the winter months and the transition to decreases in flow after spring runoff and during the summer months (Figure 2). The increases in flow in Reach 2 during the winter are largely due to inflow from the Blacksmith Fork River. The decreases in flow between gages in the summer are due primarily to the Crockett and Young Ward Canal diversions. There is also a reduction in inflow from the Blacksmith Fork due to it also experiencing many upstream diversions.

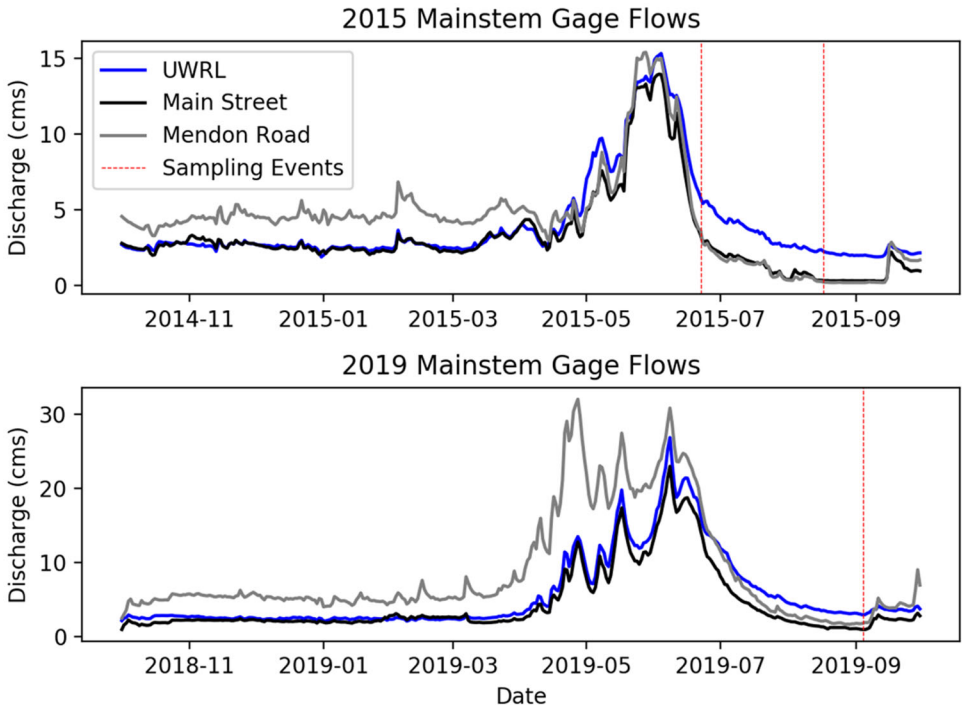

Figure 2. Discharge time series for the LRO mainstem gages at the UWRL, Main Street and Mendon Road during 2015 and 2019.

The mainstem synoptic flows for the study area focus on low flow periods and show a more detailed understanding of the overall decrease in discharge from the urban to the agricultural portion of the watershed (Figure 3a). The largest decrease in flow in the upstream portion of the urban section in each sampling event is again due to the Crocket Canal diversion. The second largest decrease in flow is due to the Young Ward Canal. The large increase in flow at the transition from the urban section to the agricultural section is due to the Blacksmith Fork and Spring Creek tributaries. Ion concentrations collected from the mainstem show a general increase as distance downstream increases (Figure 3b-3h). In general, the concentration observed at a given mainstem sampling location is the highest during the August 2015 sampling event, and the lowest during the June 2015 sampling event. This temporal trend is inversely correlated with streamflow. The ungaged inflows generally have a higher ion concentration in the agricultural area relative to the urban area (Figure 4). The ion concentrations are also generally inversely correlated with streamflow for each of the three sampling events.

3.2 HCA Results

For some of the collected inflow samples (Figure 4), the primary source of the inflow was identified as being likely groundwater or surface water based on system knowledge; other samples were known to be primarily groundwater or surface water sourced based on visual tracing. This allowed categories representative of different source types to be established. Samples could be categorized as being primarily sourced

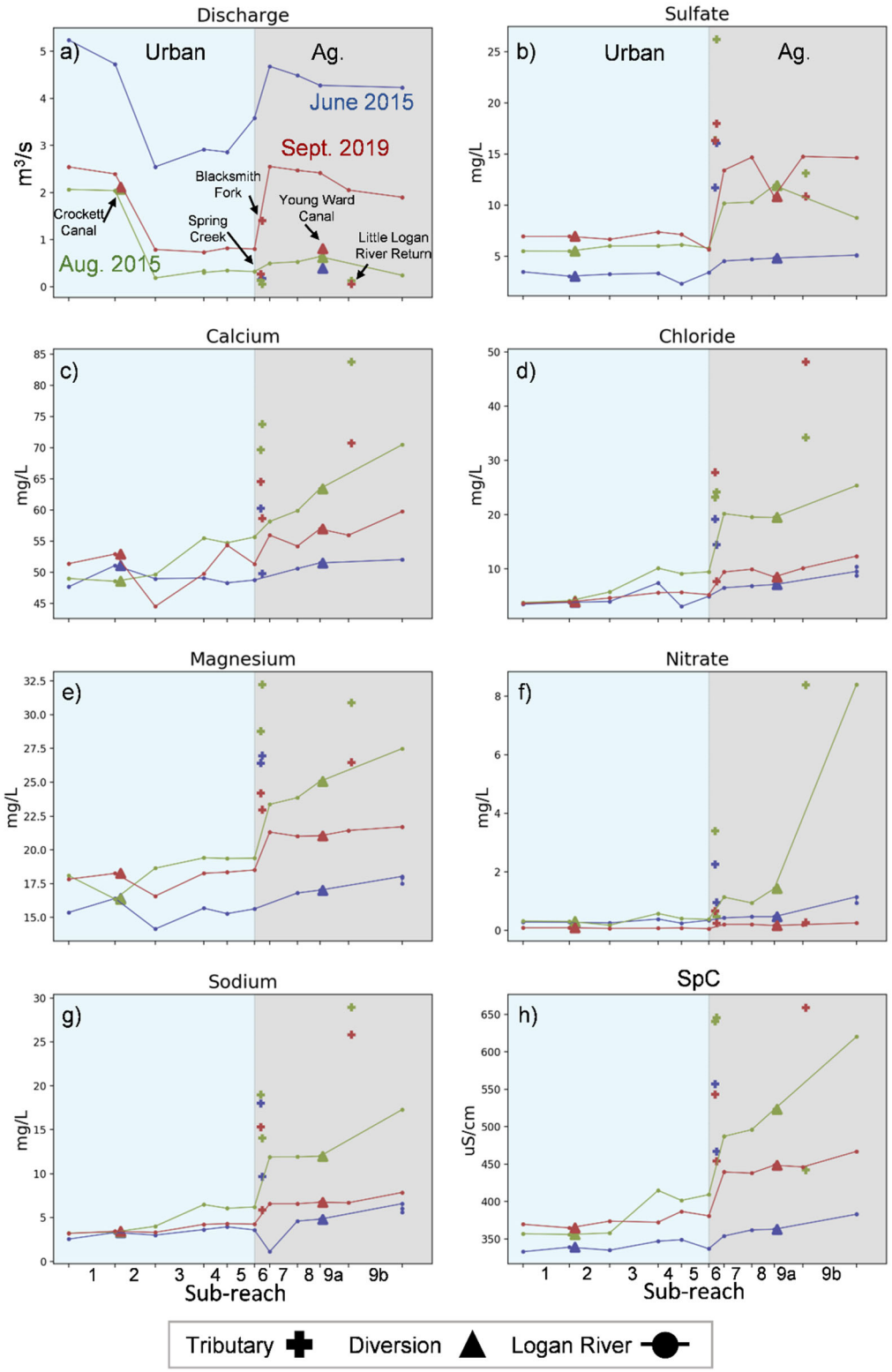

Figure 3. Main stem sampling results for June 2015, August 2015, and September 2019. Light blue background represents the urban sub-reaches and the grey background represents the agricultural sub-reaches.

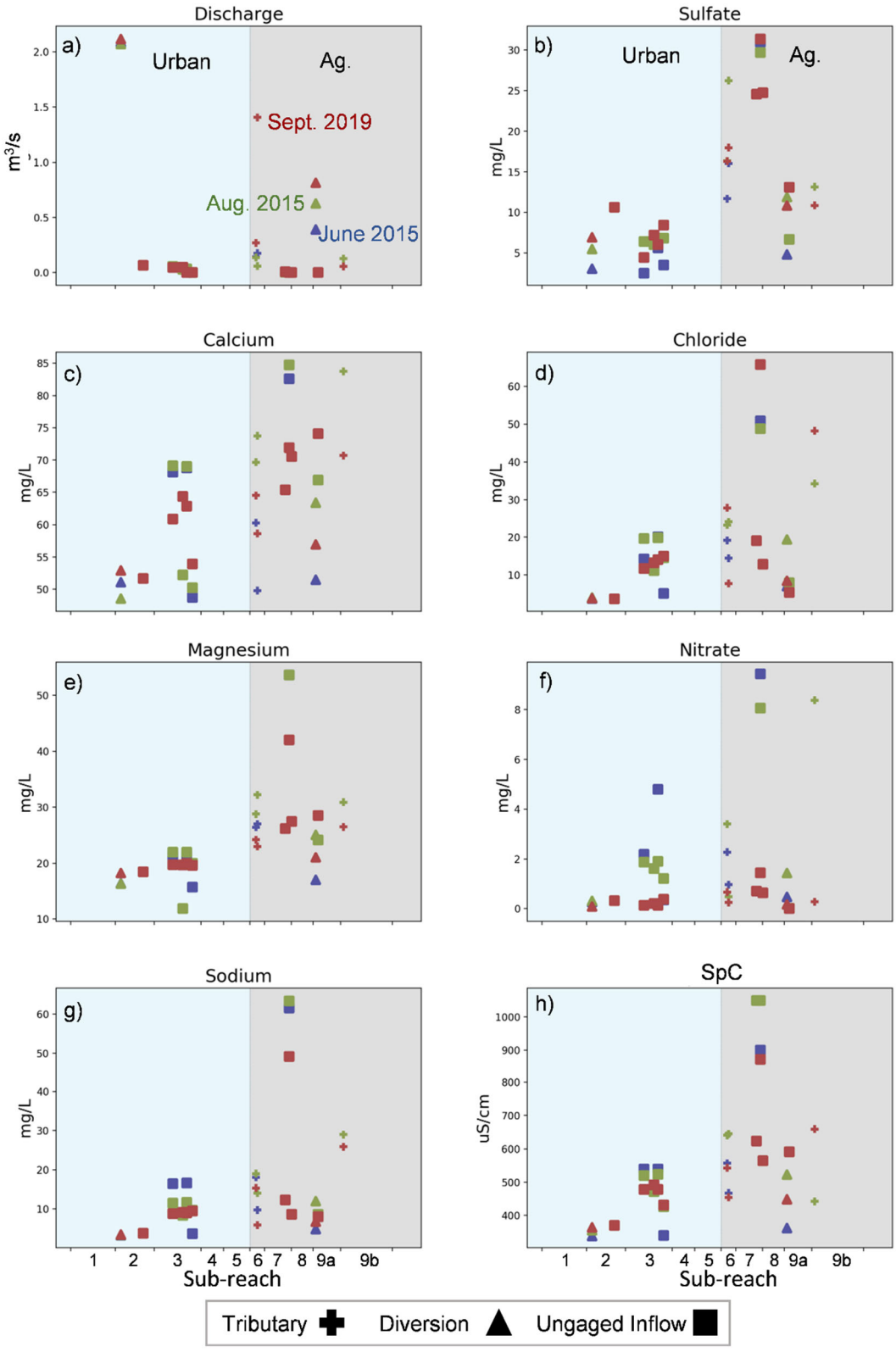

Figure 4. Chemical sampling results of tributary, diversion, and identified but ungaged inflows within the study area.

from urban surface water, urban groundwater, agricultural surface water, and agricultural groundwater (Figure 5).

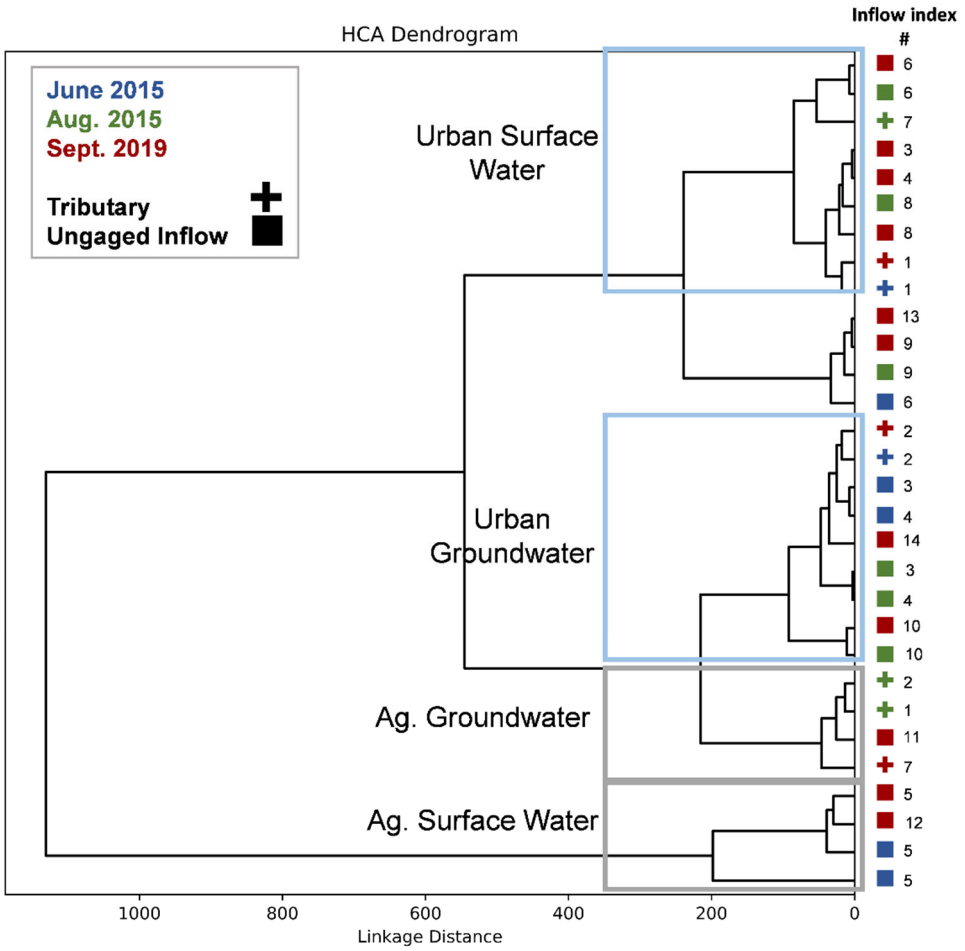

Figure 5. HCA for the composite dataset where crosses and squares represent tributary and ungaged inflows, respectively, and colors represent the different sampling dates. The light blue and grey boxes bracket the urban and agricultural sections, respectively, shown in Figure 1.

Based on local knowledge and inflow samples, the urban surface water category was representative of samples taken from canals and storm drains that are known to drain urban irrigation water. The urban groundwater category was representative of shallow groundwater flow from springs and groundwater drains in known high water table locations. The agricultural surface water category contained samples from agricultural return flows and agricultural surface runoff. Samples within the agricultural groundwater

category included samples from seeps along the river bank in the agricultural area. The four uncategorized ungaged inflow samples shown in Figure 5 were collected from irrigation returns where water traveled a relatively short distance from the point of diversion on the Logan River before being returned to the river. These samples still possessed a composition that was more similar to that of the Logan River when compared to the composite HCA categories. While most samples collected from the same location where categorized consistently between sampling events, some inflows were identified in the HCA as sourced by surface water during one sampling event and then sourced by groundwater during subsequent sampling event(s). This suggests a change in source over time (Figures A2-A4) or concentrations ranges that span two categories. This problem was most prevalent in the urban area indicating that most samples collected in the urban area contain significant portions of both surface water and groundwater. Regardless, the HCA results conducted for each event-specific set of samples yielded the same four identifiable groups (Figures A2-A4), even if some locations moved between categories. The concentration ranges for each ion derived from the HCA results (Figure 6) show that some categories had consistent concentration ranges between the event and composite HCA clustering, but others varied significantly due to certain samples being moved to another category.

3.3 Flow and Mass Balances

The net flow balance results for the stream gages using Eqn. (1) shows that the predominantly urban reach, Reach 1, experienced a net loss during most of the 2015 and 2019 water years and net losses of -8%, -3%, and -4% during the June 2015, August

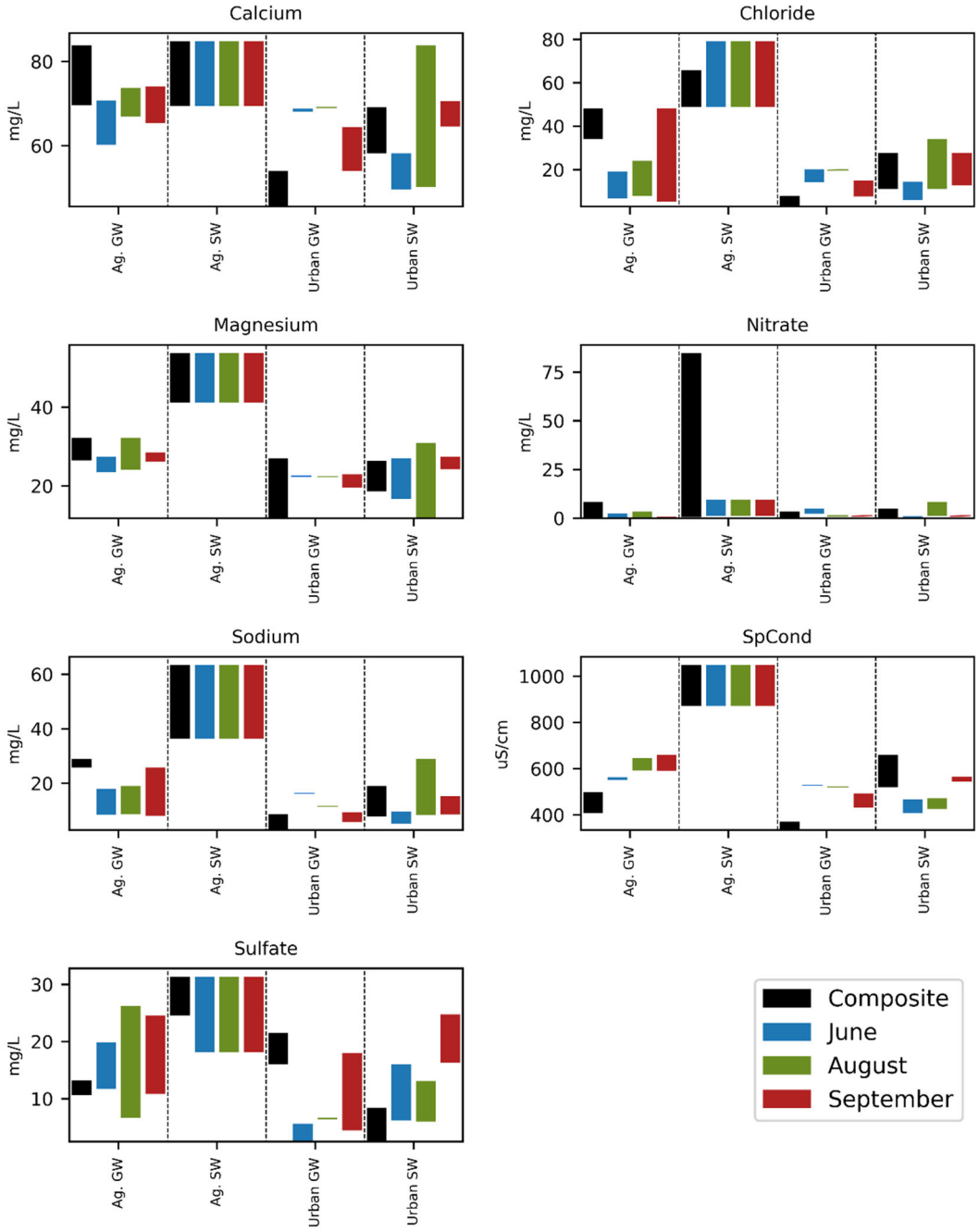

Figure 6. Ion concentration ranges of the four different source categories shown for the composite, black, June 2015, blue, August 2015, green, and September 2019, red, ion sample datasets.

2015, and September 2019 sampling events, respectively (Figure 7). The agricultural

reach, Reach 2, shows a consistent net gain during both the 2015 and 2019 water years

with relative gains of 173% and 106% during the August 2015, and September 2019 sampling events, respectively.

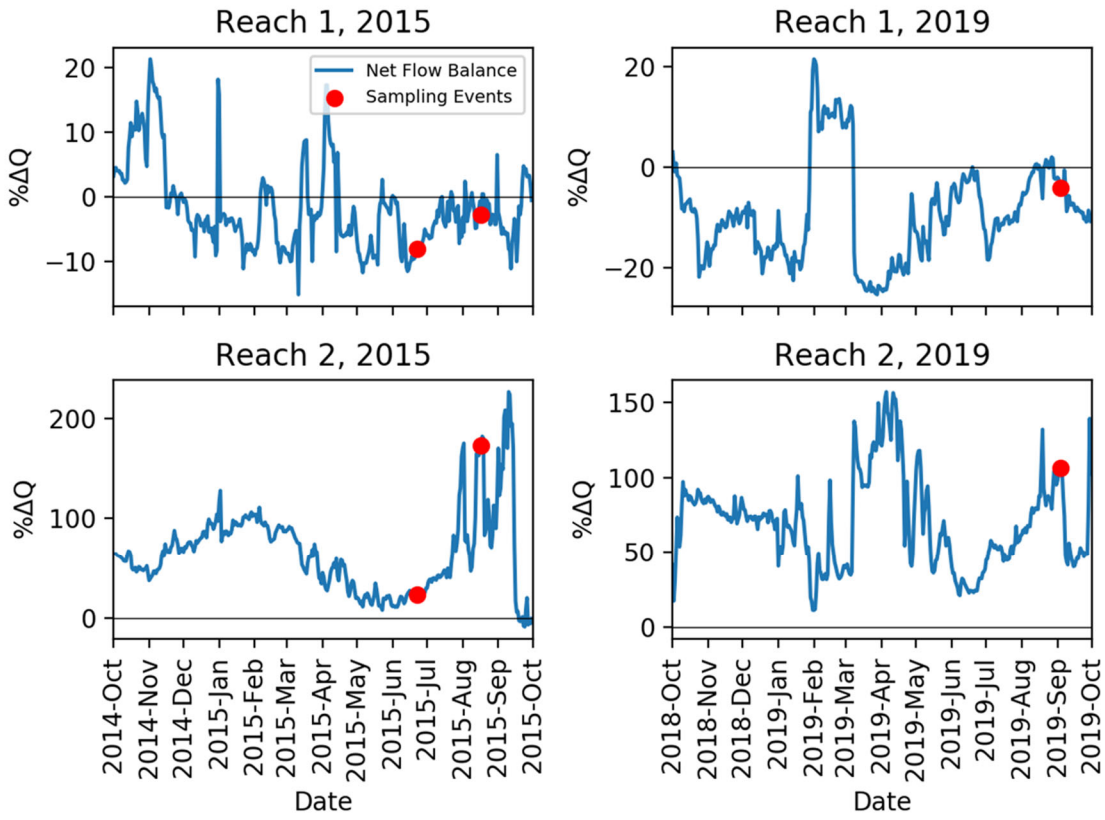

Figure 7. Net flow balance for Reach 1 and 2 for the 2015 and 2019 water years. The change in flow between gages is shown as a percentage relative to upper gage in each reach.

To gain further insight into these trends we examined the flow and mass balance results for the sub-reaches. To understand the sensitivity of the solutions for Q_{gw}, Q_{sw}, and Q_{out} to different ion pairs, the interquartile range of the solutions to the system of equations was compared across each combination of ion pairs for each sub-reach. This was done for the composite concentration ranges and the event-specific concentration ranges. As an example, Figure 8 illustrates flows as a percentage relative to the measured flow at the beginning of a sub-reach using the composite concentration ranges for Sub-

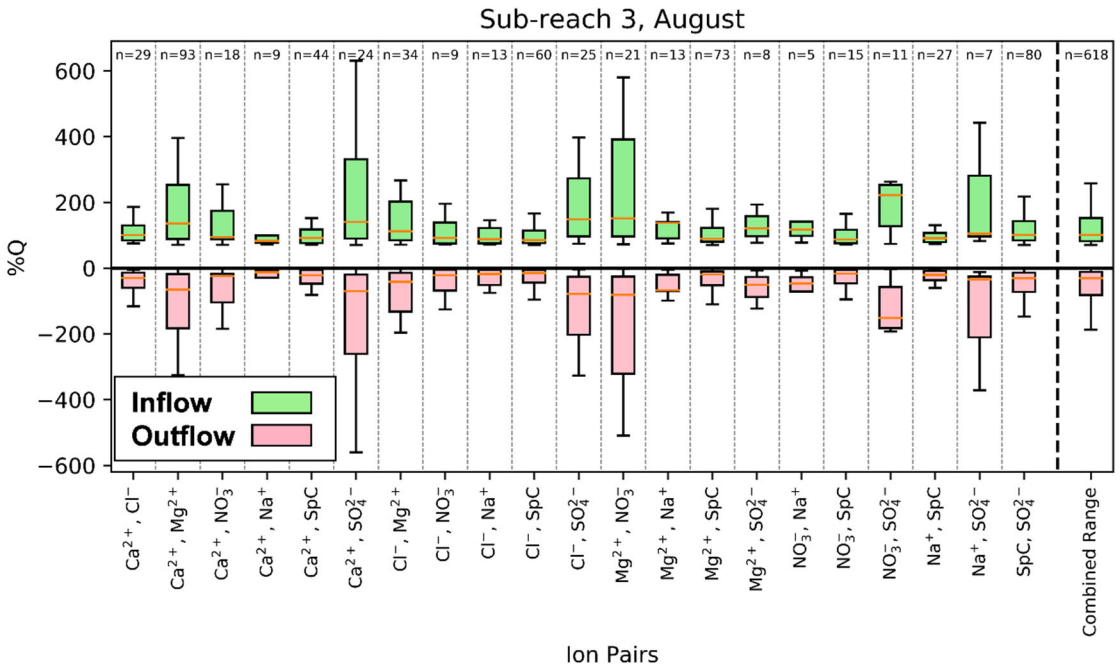

Figure 8. Comparison of flow distributions across ion pairs for Sub-reach 3 for the August 2015 sampling event. Results are shown for calculations using the composite dataset of ion samples. Red boxes represent the interquartile range of outflow within the sub-reach (Q_{out}) for a given ion pair while green boxes represent the interquartile range of the inflow within the sub-reach ($Q_{gw} + Q_{sw}$). The number of valid solutions produced by each ion pair is also shown (n). The combined range shows the inflow/outflow distribution for the sub-reach using the results from all ion pairs. Figures 9-11 present the combined range values.

reach 3 during the August 2015 sampling event. For this plot, Q_{gw} and Q_{sw} were summed together to represent the total inflow within a sub-reach. Here the number of solutions for Q_{gw}, Q_{sw}, and Q_{out} produced by an ion pair is important because a greater number of solutions for Q_{gw}, Q_{sw}, and Q_{out} are weighted more when calculating the combined median and interquartile range set for a sub-reach. For example, the ion pairs of Ca^{2+} and SO_4^{2-} and Mg^{2+} and NO_3^- produce relatively large ranges with relatively high median values; however, these ion pairs did not significantly increase the combined range and median because their counts represent a small fraction of the total 618 samples within the combined range. For some sub-reaches, very few or no solutions are provided for a given

ion pair, and in some cases, no solutions were determined for any ion pair (Figures A5-A10). The ion pairs for which solutions were determined varied between sub-reaches, suggesting the importance of using many different ions.

The combined ranges calculated for Q_{gw}, Q_{sw}, and Q_{out} in each sub-reach using the composite and event specific concentration ranges (Figures 9-11, A11-A13) provide an understanding of the information contained in the concentration ranges associated with both individual sampling events versus ranges derived from the composite dataset. For the June 2015 sampling event, notable outflow (i.e. 1st-quartile of a range had a magnitude greater than 5%) was estimated in Sub-reaches 1, 7, and 8 using both the composite and the event-specific ion concentration ranges (Figure 9). Using the composite ion range, significant groundwater inflow was estimated in Sub-reach 9, and significant surface water inflow was estimated in Sub-reach 3. In contrast, calculations with the event-specific ion dataset suggest significant groundwater inflow in Sub-reaches 1, 5, and 9, and significant surface water inflow in Sub-reach 3. When using the composite dataset concentration ranges, an insufficient number of solutions (<100) were found in sub-reach 5 and 6, and in sub-reaches 3, 4, and 6 when using the event-specific concentration ranges. These sub-reaches were removed from the final results.

For the August 2015 sampling event, significant outflow was estimated for Sub-reaches 3, 5, 6, 7, 8, and 9 when using both the event-specific and composite datasets (Figure 10). Both the composite and event-specific concentration ranges yielded significant groundwater inflow in Sub-reaches 3, 6, 7, 8, and 9, and significant surface water inflow in Sub-reach 3 and when using the composite dataset in Sub-reach 9. Using

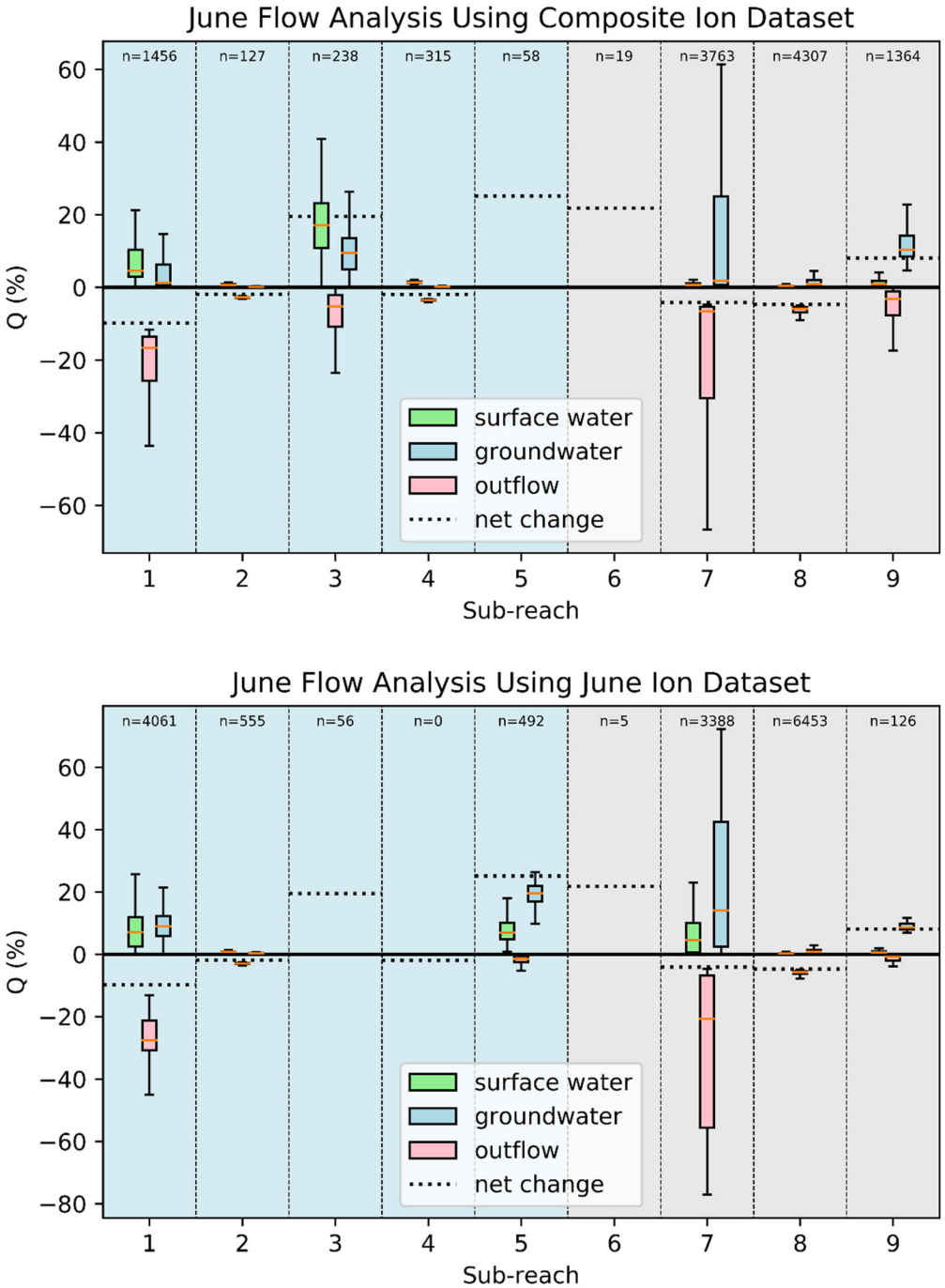

Figure 9. Results of the flow and mass balance analysis for the June 2015 sampling event for reaches with significant flow (i.e., 1st-quartile of a range had a magnitude greater than 5%). If a sub-reach had Insufficient solutions (i.e., less than 100 solutions) for Q_{gw}, Q_{sw}, and Q_{out}, boxplots are not shown. The dotted lines represent the ΔQ in each sub-reach.

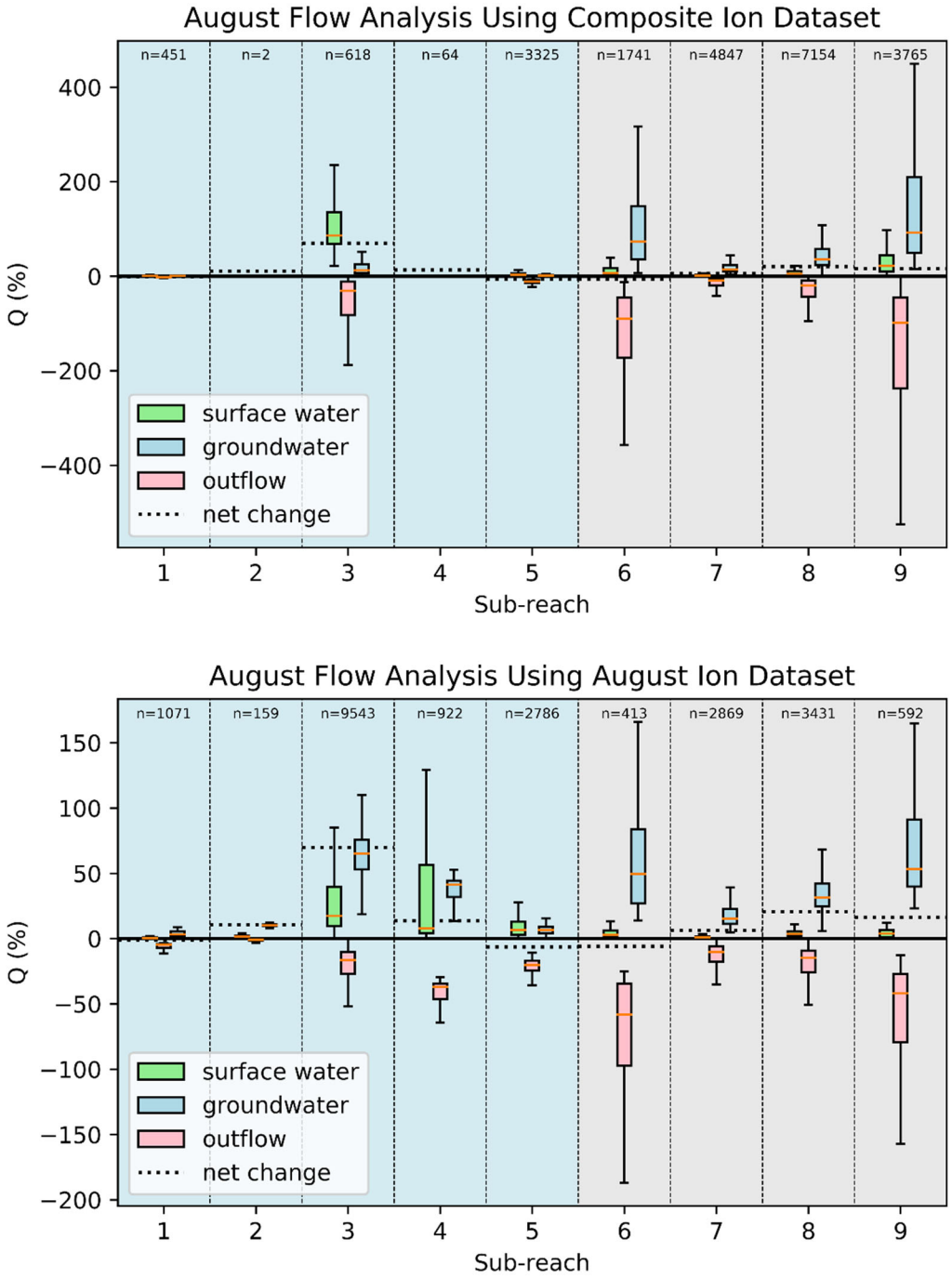

Figure 10. Results of the flow and mass balance analysis for the August 2015 sampling event for reaches with significant flow (i.e., 1st-quartile of a range had a magnitude greater than 5%). If a sub-reach had insufficient solutions (i.e., less than 100 solutions) for Q_{gw}, Q_{sw}, and Q_{out}, boxplots are not shown. The dotted lines represent the ΔQ in each sub-reach.

the composite ion dataset an insufficient number of solutions (<100) composed the ranges in sub-reaches 2 and 4. Again, these sub-reaches were removed from the final results.

For the September 2019 sampling event, significant outflow was calculated in Sub-reaches 1, 3, 7, 9a, and 9b when using both the event-specific and composite datasets (Figure 11). Significant groundwater inflow was calculated in Sub-reaches 6, 7, and 9a using the composite dataset and Sub-reaches 3, 4, 8, 9a using the event-specific datasets. Significant surface water inflow was calculated in Sub-reach 4 when using the composite ion dataset and Sub-reach 3 when using the event-specific dataset (Figure 11). Using the composite ion dataset an insufficient number of solutions (<100) composed the ranges in Sub-reaches 2 and 5, and in Sub-reaches 2, 5, and 6 when using the event-specific concentration ranges; these Sub-reaches were left out of the results.

When comparing the net change in flow between Reaches 1 and 2 calculated from the gage data (Figure 6) to the magnitude of gains and losses calculated from the sampling data (Figures 9-11), the net flow balances do not fully represent the amount of exchange occurring across the study area. Reach 1 shows a consistent net loss across all sampling events while most of the sub-reaches (Sub-reaches 1-4) received significant inflows during most sampling events (Figures 9-11). However, the losses are greater likely due to a lower groundwater table (hence loss to groundwater) and the extraction of many small water rights (Figure A1). The net flow balance shows net inflow across reach 2; however, Sub-reaches 5-9 often show outflow in addition to the large amount of inflow relative to the magnitude of streamflow in the channel.

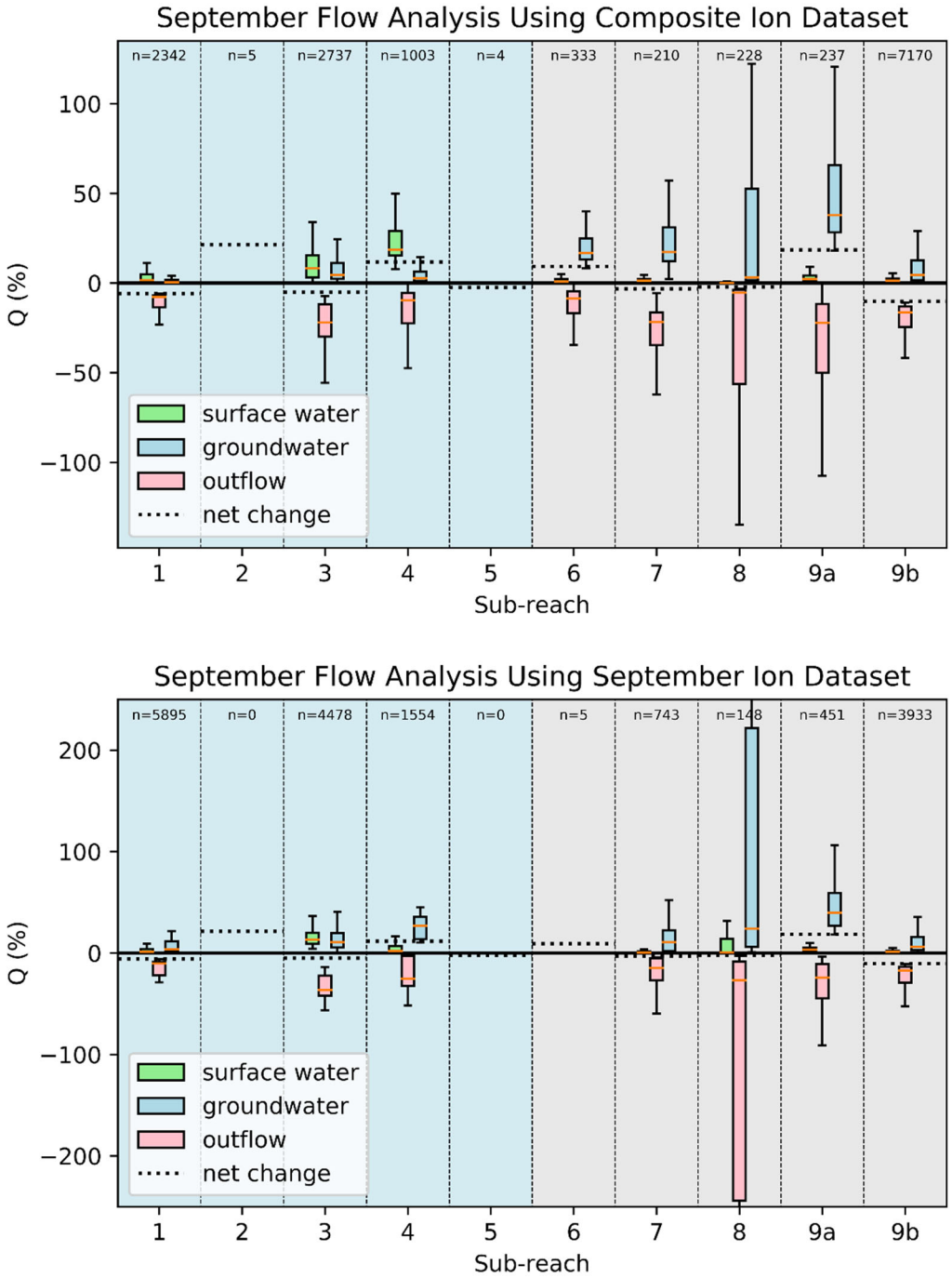

Figure 11. Results of the flow and mass balance analysis for the September 2019 sampling event for reaches with significant flow (i.e., 1st-quartile of a range had a magnitude greater than 5%). If a sub-reach had insufficient solutions (i.e., less than 100 solutions) for Q_{gw}, Q_{sw}, and Q_{out}, boxplots are not shown. The dotted lines represent the ΔQ in each sub-reach.

CHAPTER IV

DISCUSSION

4.1 Validity and Limitations of the Method

The use of clustering analysis combined with flow and mass balance equations provides a method for determining the temporal and spatial variability of groundwater and surface water inflow and outflow within urban and agricultural influenced reaches. For this method to be effective, a representative sampling of the different inflow sources to the study area is critical. For example, no samples from ungaged inflows were collected within sub-reaches 4, 5, and 6 (Figure 1). Because these sub-reaches are a transition between the urban area and the agricultural area, the ion concentrations of the inflows in these sub-reaches are likely a combination of both urban and agricultural sourced water. The lack of sampling from these sub-reaches likely contributed to: 1) the disagreement in the magnitude of inflow and outflow occurring within these sub-reaches when comparing the composite dataset to the event-specific dataset (Figures 9-11), 2) the inability to calculate some solutions for sub-reaches 4, 5 and 6 (Figures 9, 10, and 11), and 3) some variability in the categorization of sources when using different event or composite data sets.

Samples must also be collected from several known sources in order to interpret the results of the cluster analysis and establish source classification based on the clusters. Without samples of known sources, the clusters cannot be linked to the source groups (i.e., groundwater, surface water). Diverse sampling of known sources also helps determine how many groups should be represented when establishing classifications

(e.g., urban and agricultural surface water and urban and agricultural groundwater). Sampling at different flows or during different seasons can also be critical. The HCA illustrated how some locations can experience a change in source category. For example, samples from the Blacksmith Fork were classified as agricultural groundwater during the June 2015 and August 2015 sampling events due to shallow agricultural return flow, but classified as urban groundwater during the September sampling event due to runoff contributions from nearby urban influences (inflow index #1, Figures A2-A4). This transition was likely caused by the significant diversion and repeated near dewatering of the Blacksmith Fork at a number of upstream irrigation diversions during the 2015 sampling events. Identifying such changes in a source can indicate the sensitivity of a location to upstream conditions and water uses.

Urban and agricultural areas are a complex system of human-built systems that interact and interfere with underlying natural surface water and groundwater flowpaths (Kendy & Bredehoeft, 2006; Schliemann, Grevstad, & Brazeau, 2021). As discussed in Cook (2013), the accuracy of the method in this case is dependent on the ability to distinguish concentration ranges for different source categories and as discussed in Aubert et al. (2013), the observed concentrations of different ions can be time and flow dependent for a given sampling location. While an event-specific dataset will account for the spatial variability of source contributions in sampled inflows, it may be limited in the representation of sources that are not sampled. A composite dataset can be used to help account for spatial and temporal variability in inflow source composition because it represents inflow samples under multiple source flow regimes. Because it potentially represents a wider range of source flow regimes, a composite dataset can make up for the

failure of an even-specific dataset to capture variability. A robust sampling of inflows repeated for each sampling event would account variability such as that observed within the Blacksmith Fork tributary example above. Examining the behavior of the Blacksmith Fork samples in the composite dataset (inflow index #1 in Figure 5) shows that the Blacksmith Fork June 2015 and September 2019 samples are classified as urban surface water while the August 2015 sample remains consistent with the event-specific HCA results and is classified as agricultural groundwater. This indicates that the Blacksmith Fork experiences significant contributions from multiple sources. In this case study, the composite dataset showed a shift in ion concentration range for the urban surface water and urban groundwater categories indicating that the samples contained significant components of both surface water and groundwater. The changes in the samples included in each category (Figure 5 and Figures A2-A4) show how the dominant components can change between sampling events.

This method for estimating ungaged inflows and outflow across sub-reaches in a watershed could be used in any system with adequate flow and water quality data. However, inflow and mainstem water quality must be discernably different. Similarly, the HCA approach can be used to classify a broad range of inflow sources and estimate associated concentrations ranges if adequate representative samples of the different source categories are obtained.

4.2 Importance of Ungaged Inflows

The net flow balance results for Reach 1 show a consistent loss across all three sampling events, while Reach 2 shows a consistent gain. While this information is useful,

the net flow balance results do not reveal the gross inflow and outflow components in these reaches. The flow and mass balance results for the sub-reaches show that the net loss and net gain occurring across Reach 1 and Reach 2, respectively, is actually the result of a more complex system of gross gains and losses from surface water and groundwater inflows and outflows.

Due to the wide range of possible solutions produced in the flow and mass balance results, the Q_{gw}, Q_{sw}, and Q_{out} values were deemed to have a notable impact on instream flows only if the first-quartile was greater than a value of 5%. Rather than considering the entire calculated range for the Q_{gw}, Q_{sw}, and Q_{out}, simply examining the median values from the composite and event-specific calculations provides an opportunity to identify and discuss trends over time and space (Figure 12).

During the June sampling event much of the inflow occurred in the urban area (sub-reaches 1-5) with some inflow in sub-reach 9 in the agricultural section (Figure 12). This pattern is consistent with the relatively high water table post-snowmelt and at the onset of the irrigation season that resulted in inflows via a series of French drains used to lower the water table in the urban area. This increased inflow is expected because of the snowmelt driven hydrograph of the Logan River elevates the local water table in the spring and is combined with early irrigation season diversions to leaky earthen canals that run through the urban areas. The inflows from both surface and groundwater observed in sub-reach 9 is also reasonable given that the river in sub-reach 9 is incised and the local groundwater head gradient is towards the river (Figure 1). The August and September sampling events show outflows or losses occurring throughout the watershed. In the agricultural area (sub-reaches 6-9), the outflow is balanced by large inflows, primarily

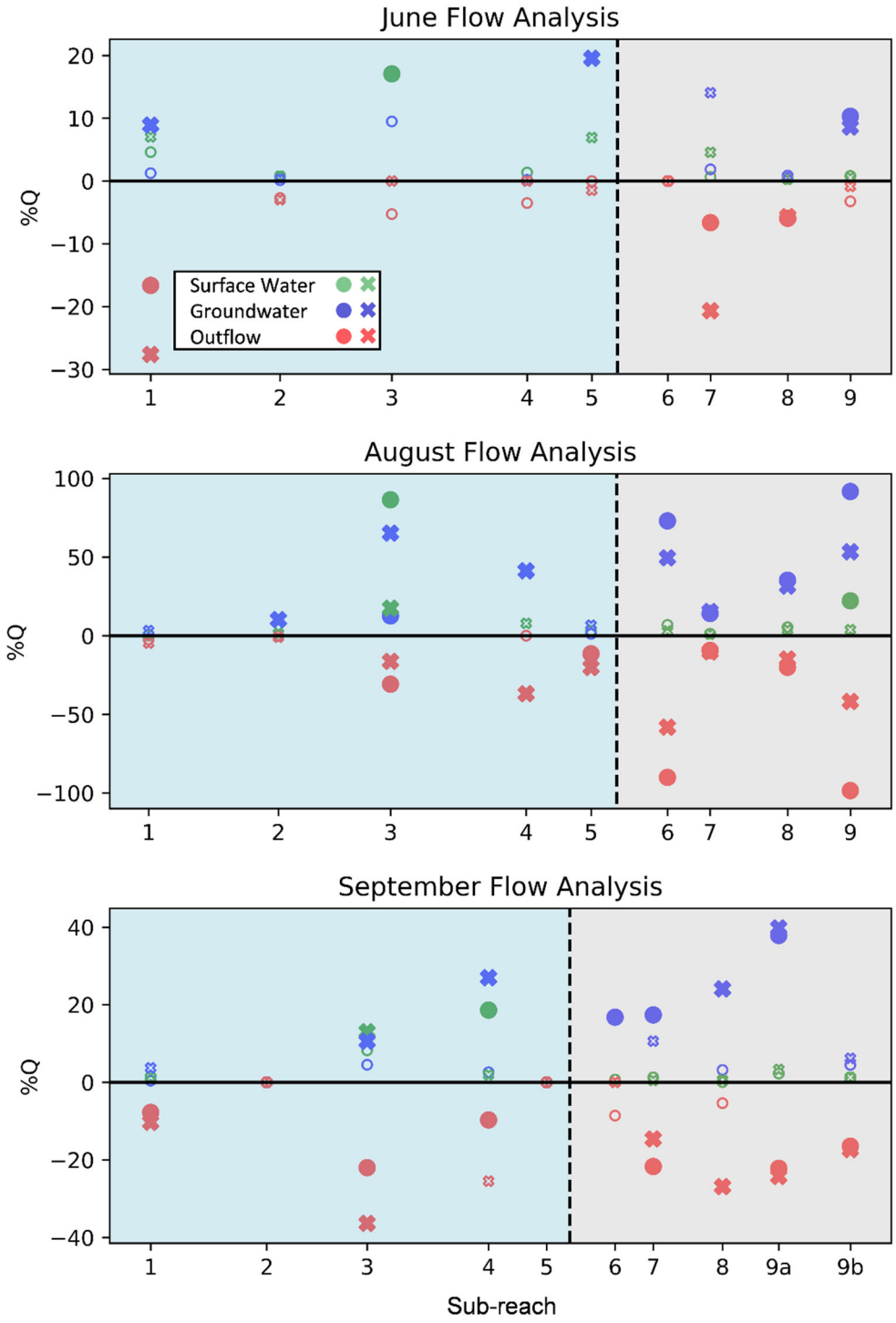

Figure 12. Plots of the median values for Q_{gw}, Q_{sw}, and Q_{out} as percentages for the June 2015, August 2015, and September 2019 flow analyses. Circles represent the results derived using composite ion dataset and the Xs represent the event-specific results. Filled shapes represent values where the 1st-quartile of the total range had a magnitude greater than 5% (or notably greater than zero) while hollow shapes represent values that are likely no different than zero.

from groundwater, to produce notable net gains (Figure 12). This is consistent with others that have found increased base flow from sub-surface inflow due to agricultural irrigation practices (Kendy & Bredehoeft, 2006; Potter, 1991). Importantly, findings like this could not be made with the net flow balance results using the mainstem gage data alone (Figure 2) because any gains are offset by the Young Ward diversion. The groundwater inflow during the August and September sampling events in sub-reach 9 replaced the water diverted by the Young Ward Canal (Figure 3a) while also accounting for the outflow that is distributed across the sub-reach. While the net flow balance reveals the large inflow occurring in sub-reach 9, it does not account for the inflow component that is offsetting the significant outflow that occurs within the sub-reach.

A comparison of the composite dataset to the event-specific datasets for Q_{gw}, Q_{sw}, and Q_{out} shows that the trends in the ranges for Q_{gw}, Q_{sw}, and Q_{out} are similar across events and the determination of significant Q_{gw}, Q_{sw}, and Q_{out} occurring were generally consistent. However, the absolute values obtained for Q_{gw}, Q_{sw}, and Q_{out} in individual sub-reaches differed frequently in the urban section between the composite and event-specific datasets. This can be attributed to difference in the HCA categorization and therefore, concentration ranges, representing the urban surface water and urban groundwater between the composite and event specific datasets. Here we found that the event-specific source category ranges for urban surface water and groundwater overlap while the composite dataset ranges generally do not (Figure 6). This discrepancy is likely due to the overall lack in the number of samples collected during each sampling event and limited samples with a singular dominant contributing source in the urban section (Figures A2-A4).

4.3 Implications for Watershed Management

Future changes in water management practices and/or climate change could have adverse impacts on the current inflow/outflow dynamics of urban and agricultural rivers. Within the Intermountain West, a shift to a higher rain-to-snow ratio, is expected due to climate change (Barnett, Adam, & Lettenmaier, 2005; Das, Pierce, Cayan, Vano, & Lettenmaier, 2011; Klos, Link, & Abatzoglou, 2014). This will likely reduce the summer base flow from mountain headwaters (Foster, Bearup, Molotch, Brooks, & Maxwell, 2016; Godsey, Kirchner, & Tague, 2014a; Jenicek, Seibert, & Staudinger, 2018), limiting supply and availability in urban and agricultural areas. As supply is reduced and if the current rate of diversion is maintained or increases due to increased demand (e.g., as a result from elevated ET as temperature is projected to rise (Christensen & Lettenmaier, 2006; Milly & Dunne, 2020)), the area will become increasingly reliant on un-quantified anthropogenically influenced inflows to maintain streamflow. This is particularly important during summer months when precipitation is scarce and irrigation demand peaks.

Urban or agricultural water management strategies may unintentionally reduce the inflows that maintain current instream flow volumes. For example, the adoption of high efficiency irrigation technologies may significantly reduce shallow groundwater recharge and tailwater (i.e., excess runoff), reducing these agricultural contributions to streamflow (Grafton et al., 2018; Scott, Vicuña, Blanco-Gutiérrez, Meza, & Varela-Ortega, 2014). Similarly, stormwater treatment or engineered retention of stormwater may decrease both urban groundwater recharge and discharge and/or surface water contributions (Hale, Turnbull, Earl, Childers, & Grimm, 2014; McPhillips, Earl, Hale, & Grimm, 2019). As

exemplified in our case study, a net flow balance that only accounts for large tributaries and diversions across a reach does not effectively represent the exchanges occurring within the reach. Although ungaged inflows from urban and agricultural sources can be small in their individual magnitude, the sum of those inflows can sustain streamflow during low flow conditions, particularly in rivers with significant diversions. Therefore, future water management efforts may benefit from identifying and account for unknown or ungaged inflows and outflow in urban and agricultural areas before implementing proposed management practices.

CHAPTER V

CONCLUSIONS

In the urban and agricultural portions of the Logan River Observatory, we generally observed net losses in the urban reach and net gains in the agricultural reach when only considering data collected by stream gages in these sections. By collecting ion samples of sources representative of inflows in our study area across different flow regimes, the sources of these inflows were categorized as urban or agricultural surface water or groundwater using HCA. This led to the identification of ion concentration ranges representative of urban and agricultural surface water and groundwater. Combining these ranges with longitudinal sampling of ions and flow along the Logan River, flow and solute mass balance analyses provided ranges of surface water and groundwater inflow and outflow at the sub-reach scales. The results revealed simultaneous inflows and outflows occurring at the sub-reach scale that could not be quantified using flow balances at the reach scale. These inflows from surface water and groundwater were found in both the urban and agricultural portions of the study area. The magnitude of these observed inflows are dependent on current land cover and water management practices within each portion of the watershed. Future changes to management practices in response to changes in climate and/or anthropogenic activity could diminish ungaged inflows that are often the primary source of instream flow downstream of large irrigation diversions. Source identification and quantification of inflows will likely provide critical information for watershed management in the near future. While the approach described here for estimating ungaged inflows and outflows

was applied to agricultural and urban stream reaches, the approach could be applied in any stream reach with variable inflow sources that have adequate flow and water quality data.

CHAPTER VI

ENGINEERING SIGNIFICANCE

Identifying sources of ungaged inflows and quantifying their inflow and the loss across stream reaches has distinct engineering significance in the area of watershed management. With an expected shift to a higher rain-to-snow ratio likely to reduce summer baseflows in the West (Barnett et al., 2005; Das et al., 2011; Foster et al., 2016; Godsey, Kirchner, & Tague, 2014b; Jenicek et al., 2018; Klos et al., 2014), additional stress will be placed on already taxed water systems in urban and agricultural areas. This will potentially further increase the importance of ungaged inflows in sustaining instream flow. A failure to account for these ungaged inflows in understanding current instream flowrates may unintentionally produce management strategies that reduce these inflow volumes. These strategies can include high efficiency irrigation, stormwater treatment, or engineered retention of stormwater (Grafton et al., 2018; Hale et al., 2014; McPhillips et al., 2019; Scott et al., 2014).

The methods presented in this work would allow managers to identify stream reaches significantly impacted by ungaged inflows and outflow as well as the sources of those inflows. This creates the opportunity for more accurate accounting within flow balances utilized by water managers. For example, in the older parts of Logan City the lots are still flood irrigated using a curb-and-gutter distribution system that is sourced from the Crockett Diversion on the Logan River. The excess water and runoff from this system provide a significant source of ungaged inflows to the river that helps maintain streamflow during low flow conditions. If the portions of Logan City using flood

irrigation were to change practices to sprinkler irrigation, the volume of ungaged inflows in the urban area would significantly decrease. Using the methods in this paper sensitive reaches can be identified, and instream flows can more easily be maintained to prevent dewatering during low-flow conditions. While this work deals with quantifying ungaged inflows and losses in urban and agricultural environments, the methods described are applicable to any stream system assuming a significant difference between instream and inflow constituent concentrations are present.

REFERENCES

Aubert, A. H., Gascuel-Odoux, C., Gruau, G., Akkal, N., Faucheux, M., Fauvel, Y., … Merot, P. (2013). Solute transport dynamics in small, shallow groundwater-dominated agricultural catchments: Insights from a high-frequency, multisolute 10 yr-long monitoring study. *Hydrology and Earth System Sciences*, *17*(4), 1379–1391. https://doi.org/10.5194/hess-17-1379-2013

Barnett, T. P., Adam, J. C., & Lettenmaier, D. P. (2005). Potential impacts of a warming climate on water availability in snow-dominated regions. *Nature*, *438*(7066), 303–309. https://doi.org/10.1038/nature04141

Bhaskar, A. S., & Welty, C. (2001). *Water Balances along an Urban-to-Rural Gradient of Metropolitan Baltimore, 2001–2009*. *XVIII*(1), 37–50.

Bhaskar, A. S., & Welty, C. (2012). Water balances along an urban-to-rural gradient of metropolitan baltimore, 2001-2009. *Environmental and Engineering Geoscience*, *18*(1), 37–50. https://doi.org/10.2113/gseegeosci.18.1.37

Christensen, N., & Lettenmaier, D. P. (2006). A multimodel ensemble approach to assessment of climate change impacts on the hydrology and water resources of the Colorado River basin. In *European Geosciences Union* (Vol. 3). Retrieved from www.hydrol-earth-syst-sci-discuss.net/3/3727/2006/

Claessens, L., Hopkinson, C., Rastetter, E., & Vallino, J. (2006). Effect of historical changes in land use and climate on the water budget of an urbanizing watershed. *Water Resources Research*, *42*(3). https://doi.org/10.1029/2005WR004131

Cook, P. G. (2013). Estimating groundwater discharge to rivers from river chemistry surveys. *Hydrological Processes*, *27*(25), 3694–3707. https://doi.org/10.1002/hyp.9493

Covino, T., McGlynn, B., & Mallard, J. (2011). Stream-groundwater exchange and hydrologic turnover at the network scale. *Water Resources Research*, *47*(12). https://doi.org/10.1029/2011WR010942

Das, T., Pierce, D. W., Cayan, D. R., Vano, J. A., & Lettenmaier, D. P. (2011). The importance of warm season warming to western U.S. streamflow changes. *Geophysical Research Letters*, *38*(23), n/a-n/a. https://doi.org/10.1029/2011GL049660

Dover, J. H. (1995). Geologic Map of the Logan 30’ x 60’ Quadrangle Cache and Rich Counties, Utah and Lincoln and Unita Counties, Wyoming. In *United States Geological Survey*. https://doi.org/10.3133/i2210

Foster, L., Bearup, L., Molotch, N., Brooks, P., & Maxwell, R. (2016). *Energy Budget Increases Reduce Mean Streamflow More Than Snow-Rain Transitions: Using integrated modeling to isolate climate change impacts on Rocky Mountain hydrology*.

Garcia-Fresca, B. (2007). *Urban-enhanced groundwater recharge: review and case study of Austin, Texas, USA*. 19–34. https://doi.org/10.1201/9780203947050-7

Gburek, W. J., & Folmar, G. J. (1999). Flow and chemical contributions to streamflow in an upland watershed: A baseflow survey. *Journal of Hydrology*, *217*(1–2), 1–18. https://doi.org/10.1016/S0022-1694(98)00282-0

Godsey, S. E., Kirchner, J. W., & Tague, C. L. (2014a). Effects of changes in winter snowpacks on summer low flows: case studies in the Sierra Nevada, California, USA. *Hydrological Processes*, *28*(19), 5048–5064. https://doi.org/10.1002/hyp.9943

Godsey, S. E., Kirchner, J. W., & Tague, C. L. (2014b). Effects of changes in winter snowpacks on summer low flows: case studies in the Sierra Nevada, California, USA. *Hydrological Processes*, *28*(19), 5048–5064. https://doi.org/10.1002/hyp.9943

Grafton, R. Q., Williams, J., Perry, C. J., Molle, F., Ringler, C., Steduto, P., … Allen, R. G. (2018). The paradox of irrigation efficiency. *Science*, *361*(6404), 748 LP – 750. https://doi.org/10.1126/science.aat9314

Hale, R. L., Turnbull, L., Earl, S. R., Childers, D. L., & Grimm, N. B. (2014). Stormwater Infrastructure Controls Runoff and Dissolved Material Export from Arid Urban Watersheds. *Ecosystems*, *18*(1), 62–75. https://doi.org/10.1007/s10021-014-9812-2

Hastie, T., Tibshirani, R., & Friedman, J. (2009). *Springer Series in Statistics The Elements of Statistical Learning Data Mining, Inference, and Prediction*.

Jenicek, M., Seibert, J., & Staudinger, M. (2018). Modeling of Future Changes in Seasonal Snowpack and Impacts on Summer Low Flows in Alpine Catchments. *Water Resources Research*, *54*(1), 538–556. https://doi.org/10.1002/2017WR021648

Jones, A. S., Aanderud, Z. T., Horsburgh, J. S., Eiriksson, D. P., Dastrup, D., Cox, C., … Baker, M. A. (2017). Designing and Implementing a Network for Sensing Water Quality and Hydrology across Mountain to Urban Transitions. *JAWRA Journal of the American Water Resources Association*, *53*(5), 1095–1120. https://doi.org/10.1111/1752-1688.12557

Kendy, E., & Bredehoeft, J. D. (2006). Transient effects of groundwater pumping and surface-water-irrigation returns on streamflow. *Water Resources Research*, *42*(8). https://doi.org/10.1029/2005WR004792

Klos, P. Z., Link, T. E., & Abatzoglou, J. T. (2014). Extent of the rain-snow transition zone in the western U.S. under historic and projected climate. *Geophysical Research Letters*, *41*(13), 4560–4568. https://doi.org/10.1002/2014GL060500

Liu, F., Wang, S., Yeh, T. J., Zhen, P., Wang, L., & Shi, L. (2020). Using multivariate statistical techniques and geochemical modelling to identify factors controlling the evolution of groundwater chemistry in a typical transitional area between Taihang Mountains and North China Plain. *Hydrological Processes*, hyp.13701. https://doi.org/10.1002/hyp.13701

McCallum, J. L., Cook, P. G., Berhane, D., Rumpf, C., & McMahon, G. A. (2012). Quantifying groundwater flows to streams using differential flow gaugings and water chemistry. *Journal of Hydrology*, *416–417*, 118–132. https://doi.org/10.1016/j.jhydrol.2011.11.040

McPhillips, L. E., Earl, S. R., Hale, R. L., & Grimm, N. B. (2019). Urbanization in Arid Central Arizona Watersheds Results in Decreased Stream Flashiness. *Water Resources Research*, *55*(11), 9436–9453. https://doi.org/10.1029/2019WR025835

Milly, P. C. D., & Dunne, K. A. (2020). Colorado River flow dwindles as warming-driven loss of reflective snow energizes evaporation. *Science*, *367*(6483).

Moya, C. E., Raiber, M., Taulis, M., & Cox, M. E. (2015). Hydrochemical evolution and groundwater flow processes in the galilee and eromanga basins, great artesian Basin, Australia: A multivariate statistical approach. *Science of the Total Environment*, *508*, 411–426. https://doi.org/10.1016/j.scitotenv.2014.11.099

National Climate Data Center, NESDIS, NOAA, U. S. D. of C. (2010). Normals Annual/Seasonal Station Details: LOGAN RADIO KVNU, UT US, GHCND:USC00425182 | Climate Data Online (CDO) | National Climatic Data Center (NCDC). *NOAA's U.S. Climate Normals (1981-2010)*. Retrieved from https://www.ncdc.noaa.gov/cdo-web/datasets/NORMAL_ANN/stations/GHCND:USC00425182/detail

Neilson, B. T., Tennant, H., Stout, T. L., Miller, M. P., Gabor, R. S., Jameel, Y., … Brooks, P. D. (2018). Stream Centric Methods for Determining Groundwater Contributions in Karst Mountain Watersheds. *Water Resources Research*, *54*(9). https://doi.org/10.1029/2018WR022664

Payn, R. A., Gooseff, M. N., McGlynn, B. L., Bencala, K. E., & Wondzell, S. M. (2009). Channel water balance and exchange with subsurface flow along a mountain headwater stream in Montana, United States. *Water Resources Research*, *45*(11). https://doi.org/10.1029/2008WR007644

Peterson, R. N., Santos, I. R., & Burnett, W. C. (2010). Evaluating groundwater discharge to tidal rivers based on a Rn-222 time-series approach. *Estuarine, Coastal*

and Shelf Science, *86*(2), 165–178. https://doi.org/10.1016/j.ecss.2009.10.022

Potter, K. W. (1991). Hydrological impacts of changing land management practices in a moderate-sized agricultural catchment. *Water Resources Research*, *27*(5), 845–855. https://doi.org/10.1029/91WR00076

Rantz, S. E. (1982). *Measurement and Computation of Streamflow: Volume 1. Measurement of Stage and Discharge*.

Ryan, R. J., Welty, C., & Larson, P. C. (2010). Variation in surface water-groundwater exchange with land use in an urban stream. *Journal of Hydrology*, *392*(1–2), 1–11. https://doi.org/10.1016/j.jhydrol.2010.06.004

Scanlon, B. R., Jolly, I., Sophocleous, M., & Zhang, L. (2007). Global impacts of conversions from natural to agricultural ecosystems on water resources: Quantity versus quality. *Water Resources Research*, *43*(3). https://doi.org/10.1029/2006WR005486

Schliemann, S. A., Grevstad, N., & Brazeau, R. H. (2021). Water quality and spatio-temporal hot spots in an effluent-dominated urban river. *Hydrological Processes*, *35*(1), e14001. https://doi.org/10.1002/hyp.14001

Schmadel, N. M., Neilson, B. T., & Kasahara, T. (2014). Deducing the spatial variability of exchange within a longitudinal channel water balance. *Hydrological Processes*, *28*(7), 3088–3103. https://doi.org/10.1002/hyp.9854

Scott, C. A., Vicuña, S., Blanco-Gutiérrez, I., Meza, F., & Varela-Ortega, C. (2014). Irrigation efficiency and water-policy implications for river basin resilience. *Hydrol. Earth Syst. Sci*, *18*, 1339–1348. https://doi.org/10.5194/hess-18-1339-2014

Spangler, L. E. (2001). *Delineation of Recharge Areas for Karst Springs in Logan Canyon, Bear River Range, Northern Utah*. Retrieved from http://utdmp.utsnow.nrcs.usda.gov

Tesoriero, A. J., Duff, J. H., Saad, D. A., Spahr, N. E., & Wolock, D. M. (2013). Vulnerability of Streams to Legacy Nitrate Sources. *Environmental Science & Technology*, *47*(8), 3623–3629. https://doi.org/10.1021/es305026x

U.S. Geological Survey. (2020). National Water Information System data available on the World Wide Web (USGS Water Data for the Nation). Retrieved from https://waterdata.usgs.gov/usa/nwis/uv?site_no=10109000

USDA Natural Resources Conservation Service. (2020). SNOwpack TELemetry Network (SNOTEL) | Tony Grove Lake (823) Utah SNOTEL Site. Retrieved January 22, 2021, from Ag Data Commons website: https://data.nal.usda.gov/dataset/snowpack-telemetry-network-snotel

Utah Division of Water Rights. (2020). Utah Points of Diversion. Retrieved August 26, 2020, from https://www.arcgis.com/sharing/rest/content/items/5d530e62e6ca42528dd13e0a453a3b73/info/metadata/metadata.xml?format=default&output=html

Utah Division of Water Rights. (2021a). Logan River 8th Ward Canal (Crockett Canal) Realtime Flow Records. Retrieved from https://waterrights.utah.gov/cgi-bin/dvrtview.exe?Modinfo=StationView&STATION_ID=56&RECORD_YEAR=2021&QuitKey=Close

Utah Division of Water Rights. (2021b). Lower Bear River Young Ward Realtime Flow Records.

Van Meter, K. J., & Basu, N. B. (2015). Catchment Legacies and Time Lags: A Parsimonious Watershed Model to Predict the Effects of Legacy Storage on Nitrogen Export. *PLOS ONE*, *10*(5), e0125971. https://doi.org/10.1371/journal.pone.0125971

Wang, D., & Cai, X. (2009). Detecting human interferences to low flows through base flow recession analysis. *Water Resources Research*, *45*(7). https://doi.org/10.1029/2009WR007819

Ward, J. H. (1963). Hierarchical Grouping to Optimize an Objective Function. *Journal of the American Statistical Association*, *58*(301), 236–244. https://doi.org/10.1080/01621459.1963.10500845

Winter, T. C. (1995). Recent advances in understanding the interaction of groundwater and surface water. *Reviews of Geophysics*, *33*(S2), 985–994. https://doi.org/10.1029/95RG00115

Winter, T. C., Harvey, J. W., Franke, O. L., & Alley, W. M. (1998). *Ground Water U . S . Geological Survey Circular 1139*.

APPENDIX

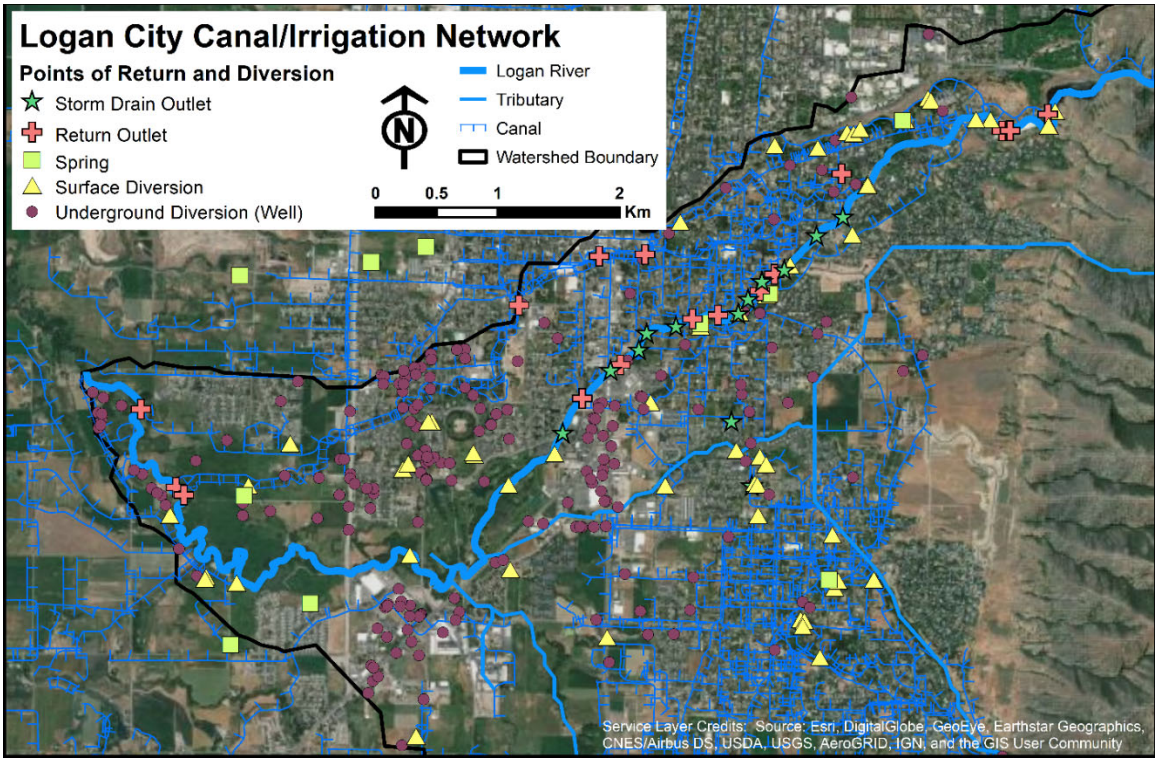

Figure A1. Logan River watershed canal and irrigation network showing the points of diversion and return based on active water right claims and Cache County Canal mapping.

Table A1. Logan River watershed gages and collected parameters.

Site Name	Reporting Agency	Updates	Water Temperature (C)	Specific Conductance (uS/cm)	pH	Dissolved Oxygen (optical, local % saturation and mg/L)	Turbidity (NTU)	Gage Height (cm)	Water Surface Elevation (m, with respect to benchmark)	Discharge (cms)
Logan River Sites										
Logan River near Franklin Basin	LRO	Continuously	•	•	•	•	•	•	•	•
Logan River near Tony Grove	LRO	Continuously	•	•	•	•	•	•	•	•
Logan River Above Wood Camp	LRO	Periodically	•	•				•	•	•
Logan River at Wood Camp Bridge	LRO	Periodically	•	•				•	•	•
Logan River at Guinavah Campground Bridge	LRO	Periodically	•	•				•	•	•
USGS at First Dam	USGS	Continuously						•		•
Logan River at the Utah Water Research Laboratory west bridge	LRO	Continuously	•	•	•	•	•	•	•	•
Logan River at Main Street (Highway 89/91) Bridge	LRO	Continuously	•	•	•	•	•	•	•	•
Logan River at Mendon Road (600 South)	LRO	Continuously	•	•	•	•	•	•	•	•
Tributary Sites										
Beaver Creek	LRO	Periodically	•	•				•	•	•
Temple Fork Outlet	LRO	Periodically	•	•				•	•	•
Ricks Spring	LRO	Periodically	•	•				•	•	•
Right Hand Fork	LRO	Periodically	•	•				•	•	•
Spring Creek above confluence with Logan River	LRO	Continuously	•	•				•	•	•
Blacksmith Fork above confluence with Logan River	LRO	Continuously	•	•	•	•	•	•	•	•
Canal Sites										
USGS at Highline Canal	USGS	Continuously						•		•
DWRi at Crocektt Canal	DWRi	Continuously								•
DWRi at Young Ward Canal	DWRi	Continuously								•
Northwest Field Canal at 1600 North	LRO	Continuously	•	•	•	•	•	•	•	•
South Logan Benson Canal at Airport Rd Pumping Station	LRO	Continuously	•	•	•	•	•			•
Storm Drain Site										
River Heights Bridge Storm Drain	LRO	Continuously	•							•

†• indicate that data are presently being collected for this parameter; Continuously = real-time updates of data online and publicly available; Periodically = periodic downloads of sensors with data posted and publicly available.

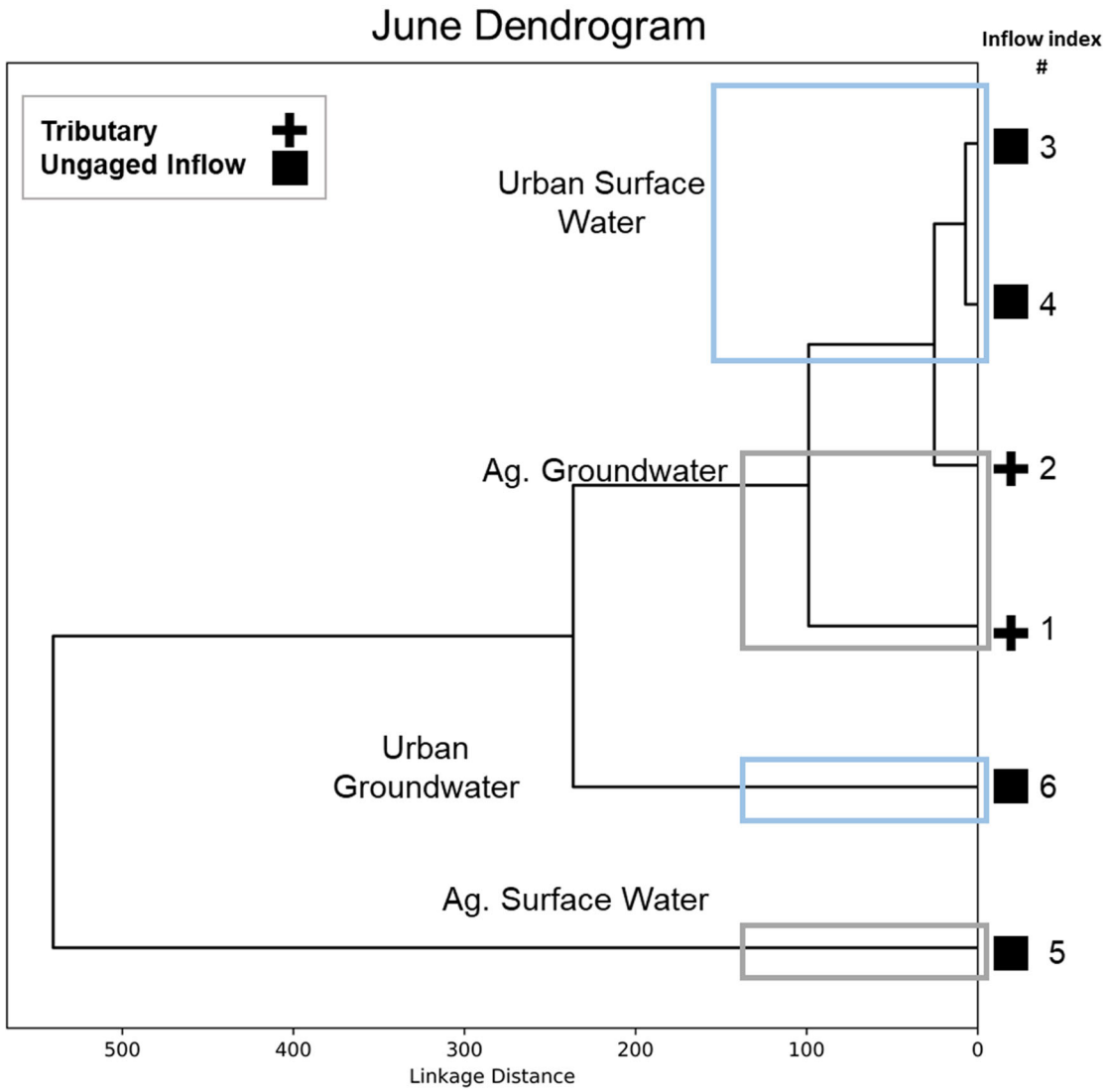

Figure A2. HCA for the June 2015 event-specific ion dataset where crosses and squares represent tributary and ungaged inflows, respectively. The light blue and grey boxes bracket the urban and agricultural sections, respectively, shown in Figure 1.

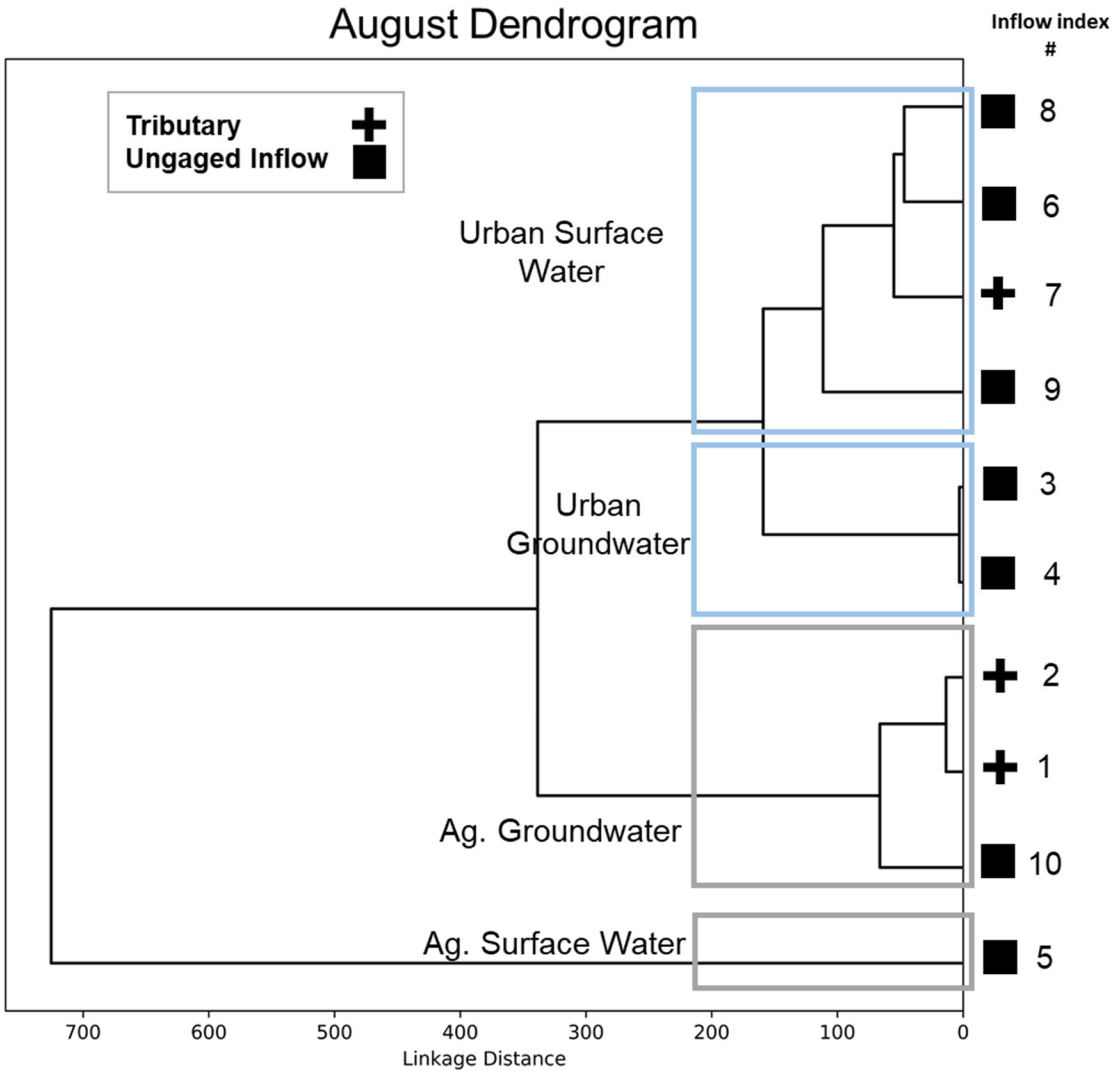

Figure A3. HCA for the August 2015 event-specific ion dataset where crosses and squares represent tributary and ungaged inflows, respectively. The light blue and grey boxes bracket the urban and agricultural sections, respectively, shown in Figure 1.

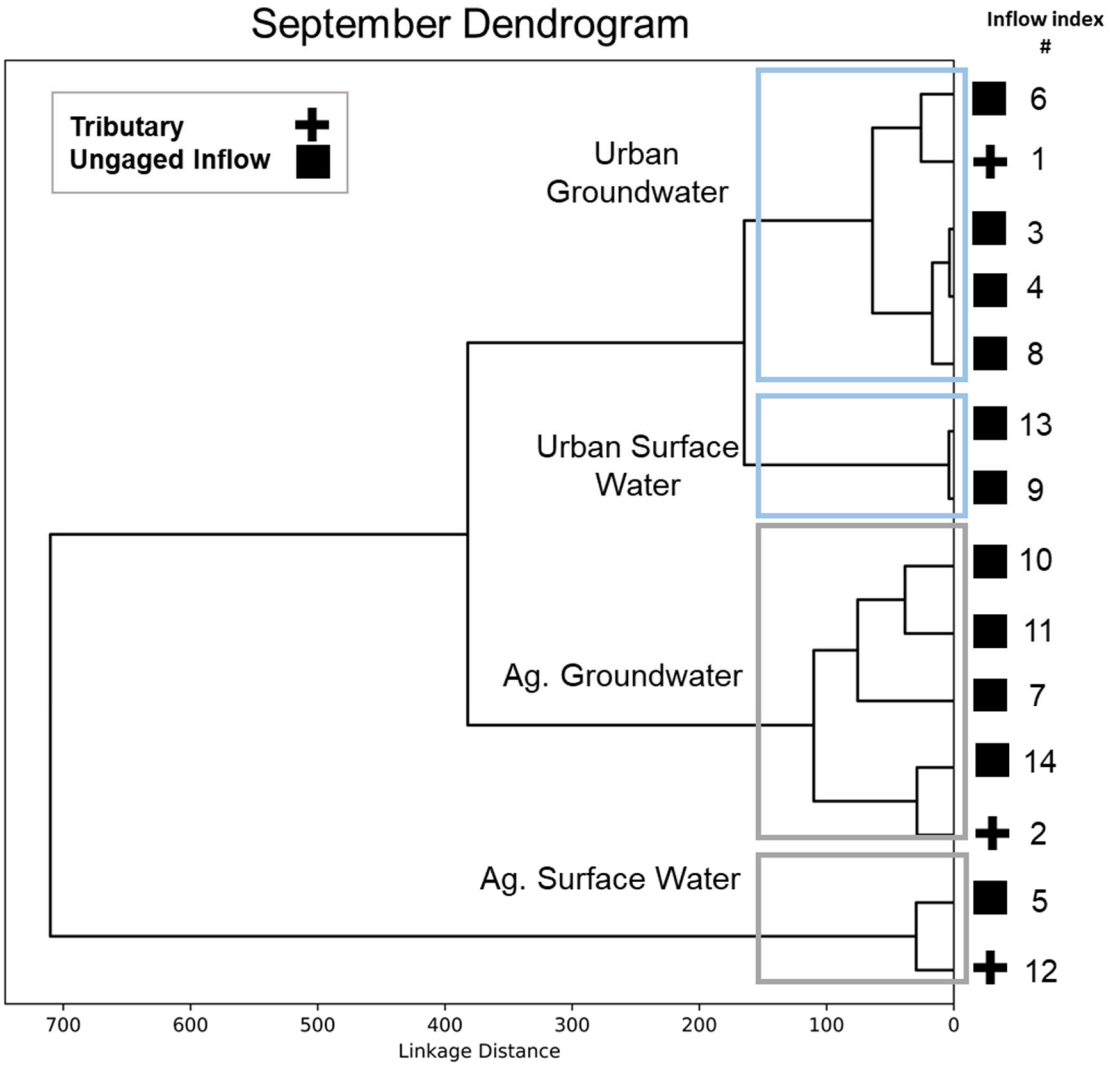

Figure A4. HCA for the September 2019 event-specific ion dataset where crosses and squares represent tributary and ungaged inflows, respectively. The light blue and grey boxes bracket the urban and agricultural sections, respectively, shown in Figure 1.

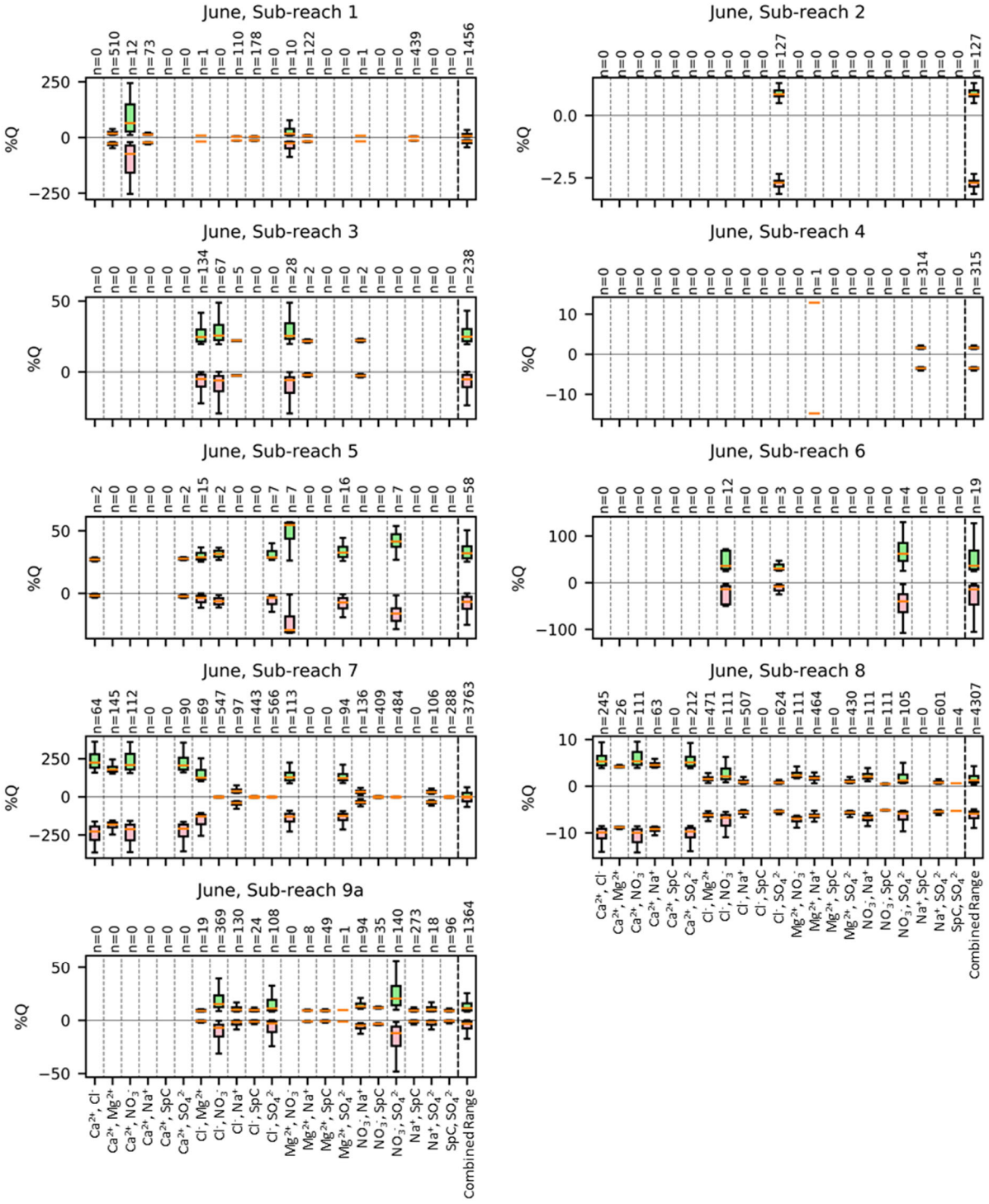

Figure A5. June 2015 composite dataset comparison of flow distributions across ion pairs for each sub-reach. Red boxes represent the interquartile range of outflow within the sub-reach (Q_{out}) for a given ion pair while green boxes represent the interquartile range of the inflow within a sub-reach ($Q_{gw} + Q_{sw}$). The inflow/outflow distribution for the sub-reach using results from all ion pairs is shown by the combined range.

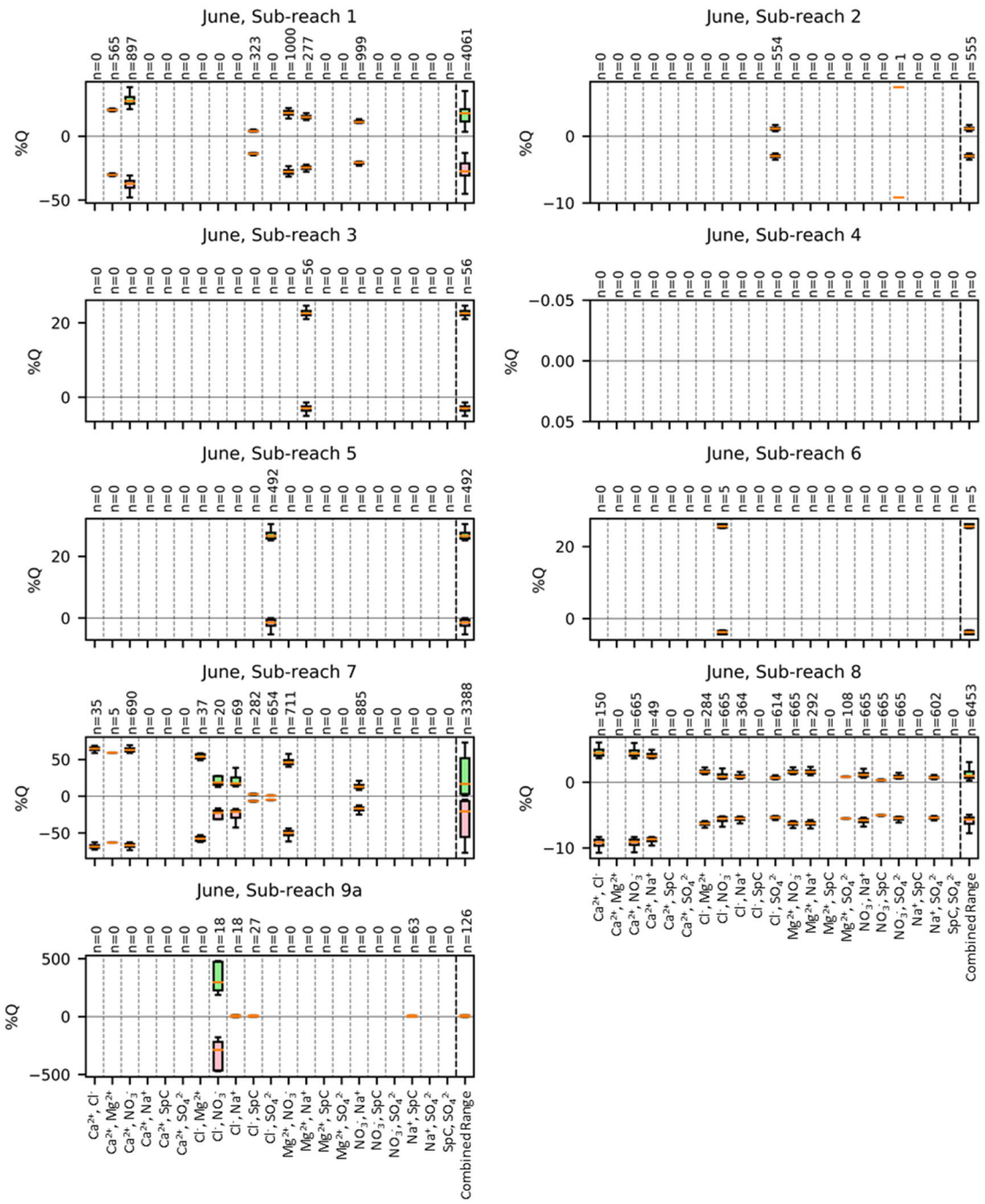

Figure A6. June 2015 event-specific dataset comparison of flow distributions across ion pairs for each sub-reach. Red boxes represent the interquartile range of outflow within the sub-reach (Q_{out}) for a given ion pair while green boxes represent the interquartile range of the inflow within a sub-reach ($Q_{gw} + Q_{sw}$). The inflow/outflow distribution for the sub-reach using results from all ion pairs is shown by the combined range.

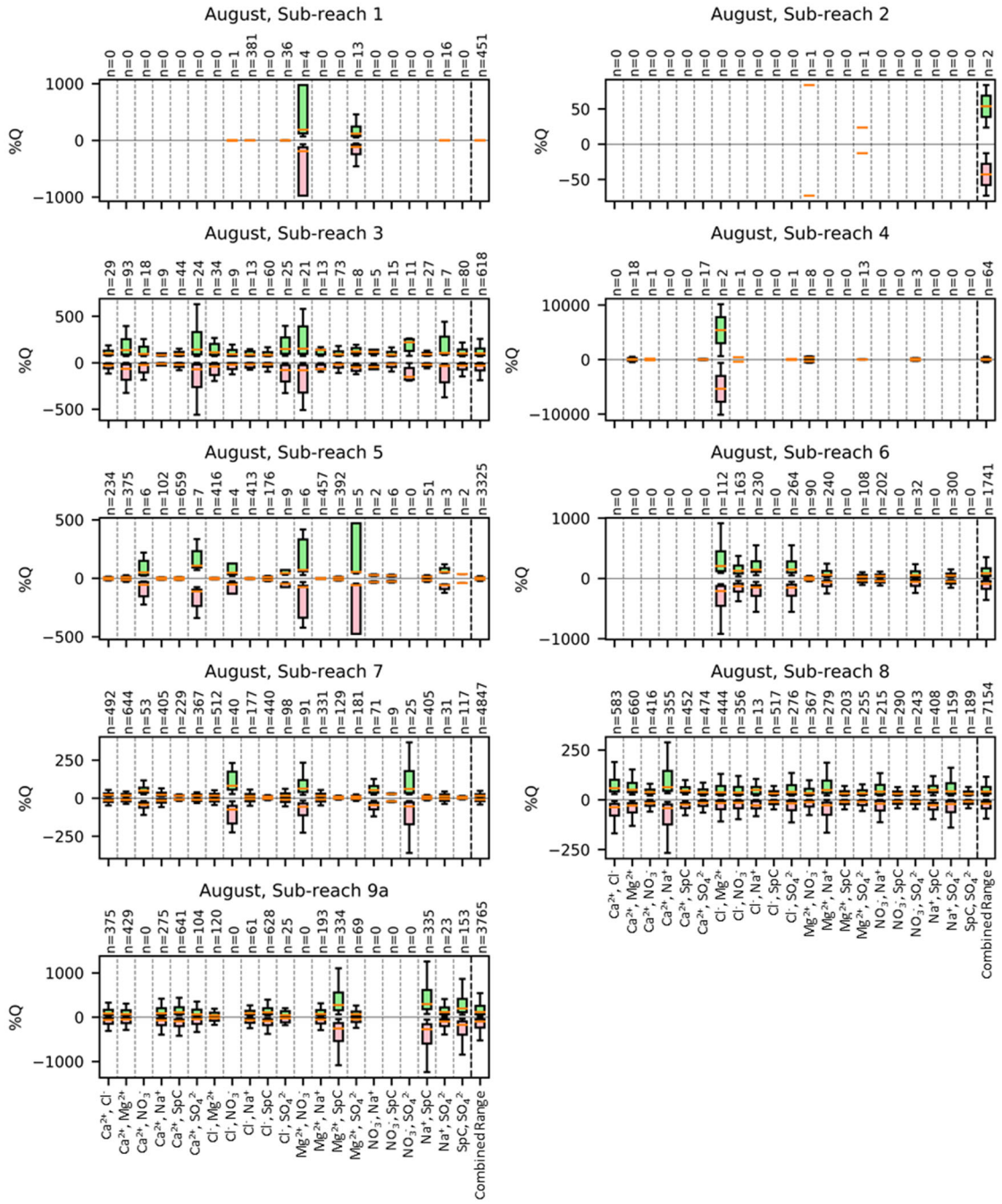

Figure A7. August 2015 composite dataset comparison of flow distributions across ion pairs for each sub-reach. Red boxes represent the interquartile range of outflow within the sub-reach (Q_{out}) for a given ion pair while green boxes represent the interquartile range of the inflow within a sub-reach ($Q_{gw} + Q_{sw}$). The inflow/outflow distribution for the sub-reach using results from all ion pairs is shown by the combined range.

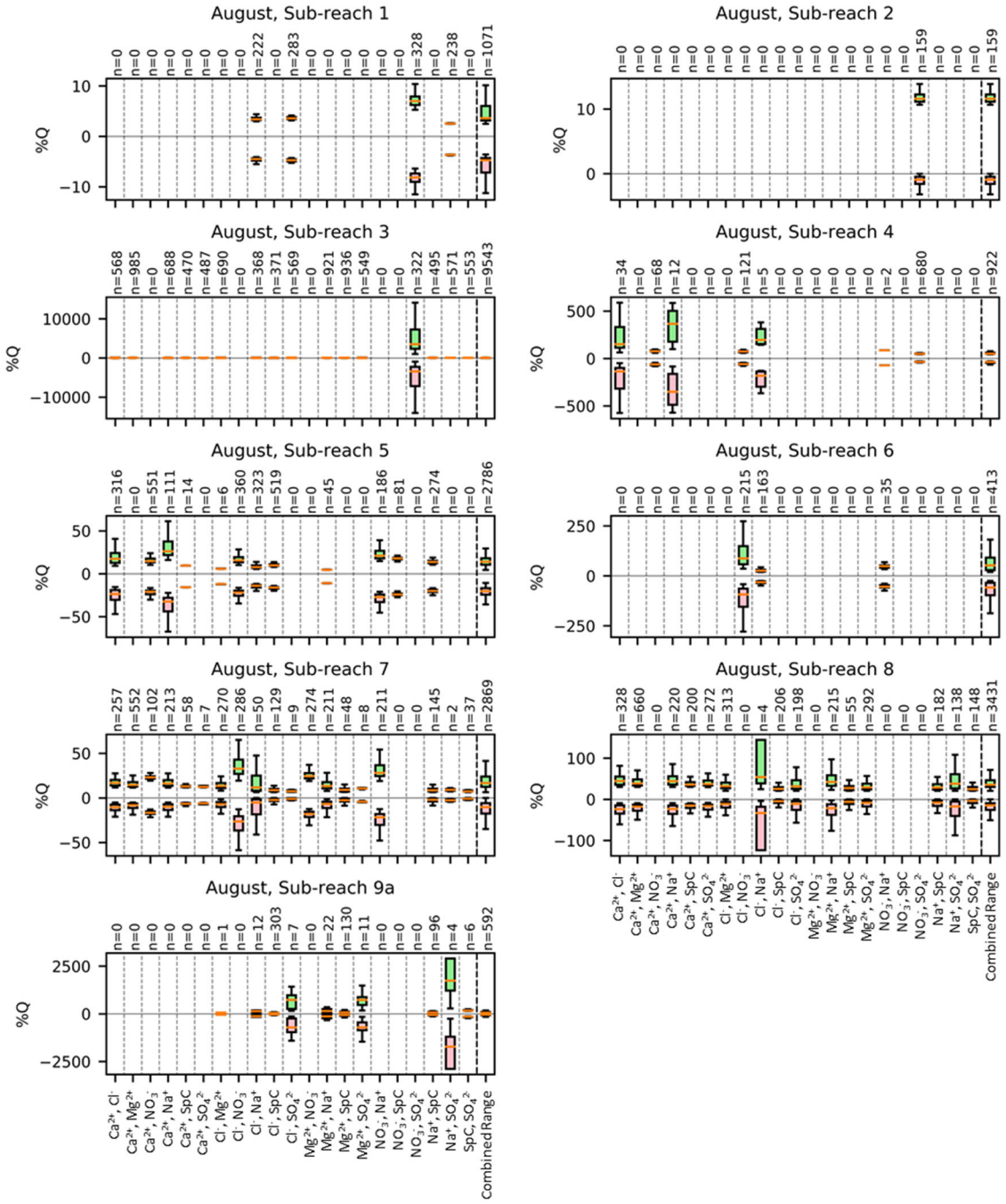

Figure A8. August 2015 event-specific dataset comparison of flow distributions across ion pairs for each sub-reach. Red boxes represent the interquartile range of outflow within the sub-reach (Q_{out}) for a given ion pair while green boxes represent the interquartile range of the inflow within a sub-reach ($Q_{gw} + Q_{sw}$). The inflow/outflow distribution for the sub-reach using results from all ion pairs is shown by the combined range.

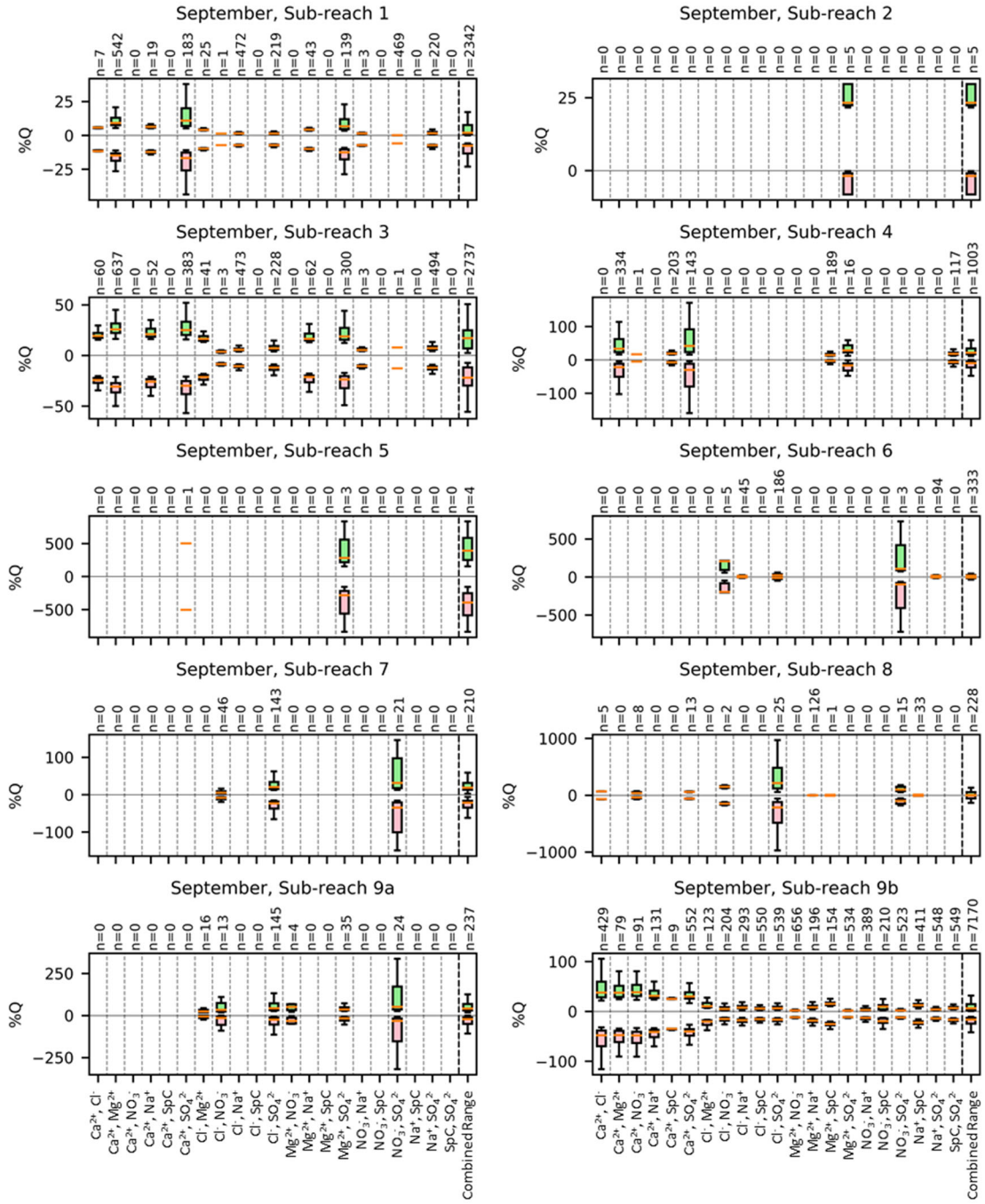

Figure A9. September 2019 composite dataset comparison of flow distributions across ion pairs for each sub-reach. Red boxes represent the interquartile range of outflow within the sub-reach (Q_{out}) for a given ion pair while green boxes represent the interquartile range of the inflow within a sub-reach ($Q_{gw} + Q_{sw}$). The inflow/outflow distribution for the sub-reach using results from all ion pairs is shown by the combined range.

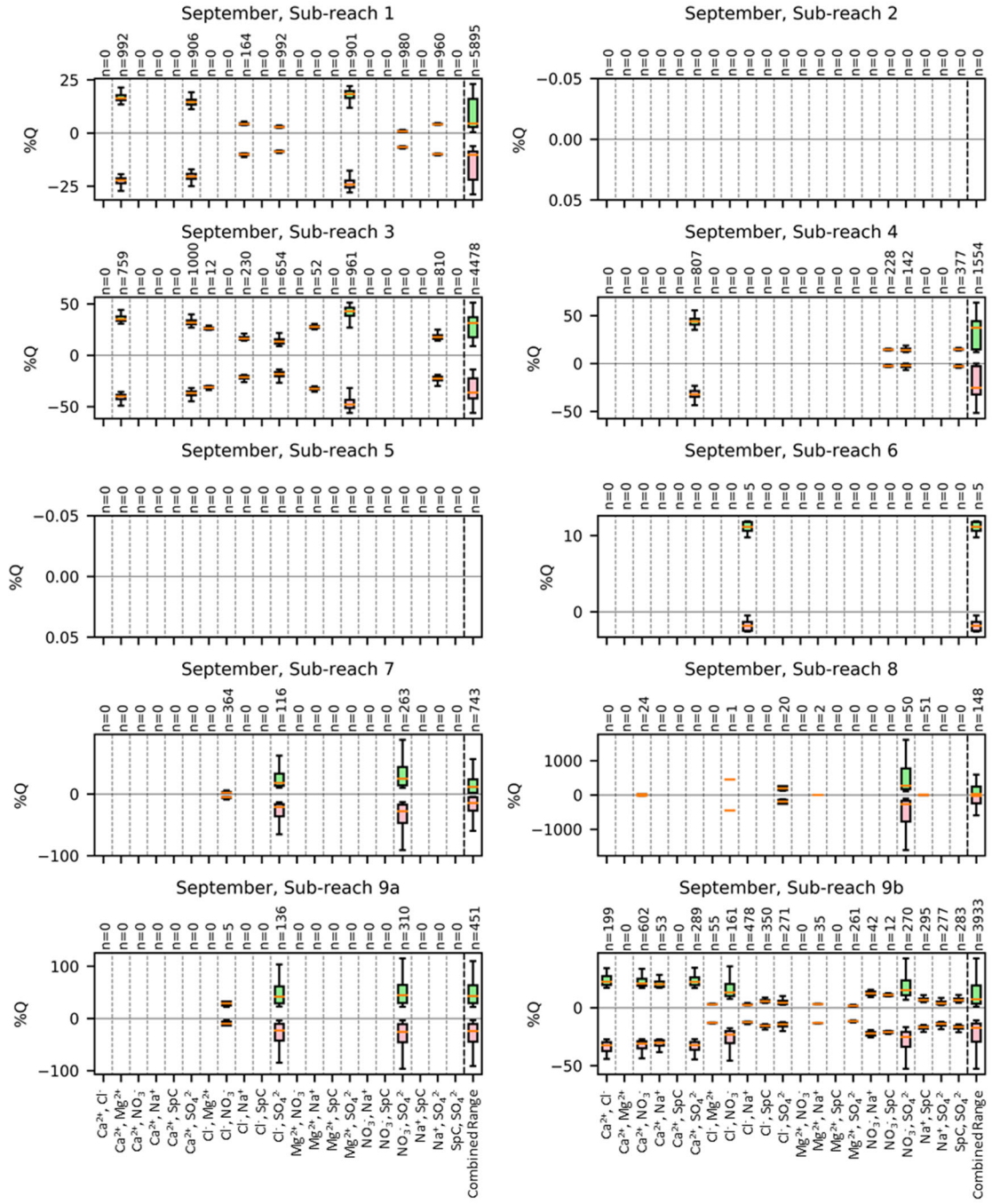

Figure A10. September 2019 event-specific dataset comparison of flow distributions across ion pairs for each sub-reach. Red boxes represent the interquartile range of outflow within the sub-reach (Q_{out}) for a given ion pair while green boxes represent the interquartile range of the inflow within a sub-reach ($Q_{gw} + Q_{sw}$). The inflow/outflow distribution for the sub-reach using results from all ion pairs is shown by the combined range.

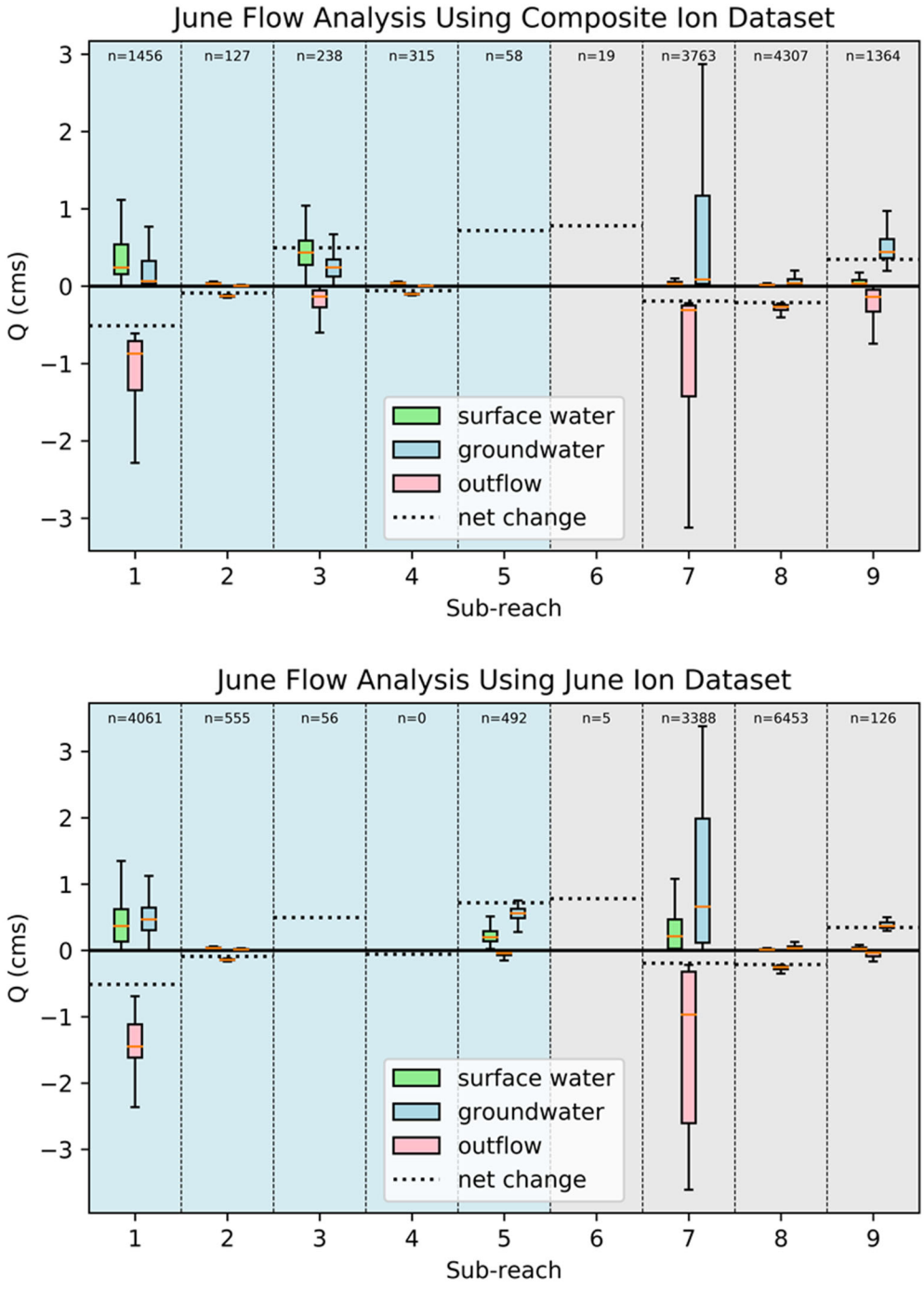

Figure A11. Results of the flow and mass balance analysis for the June 2015 sampling event for reaches with significant flow (i.e., 1st-quartile of a range had a magnitude greater than 5%). If a sub-reach had insufficient solutions (i.e., less than 100 solutions) for Q_{gw}, Q_{sw}, and Q_{out}, boxplots are not shown. The dotted lines represent the ΔQ in each sub-reach.

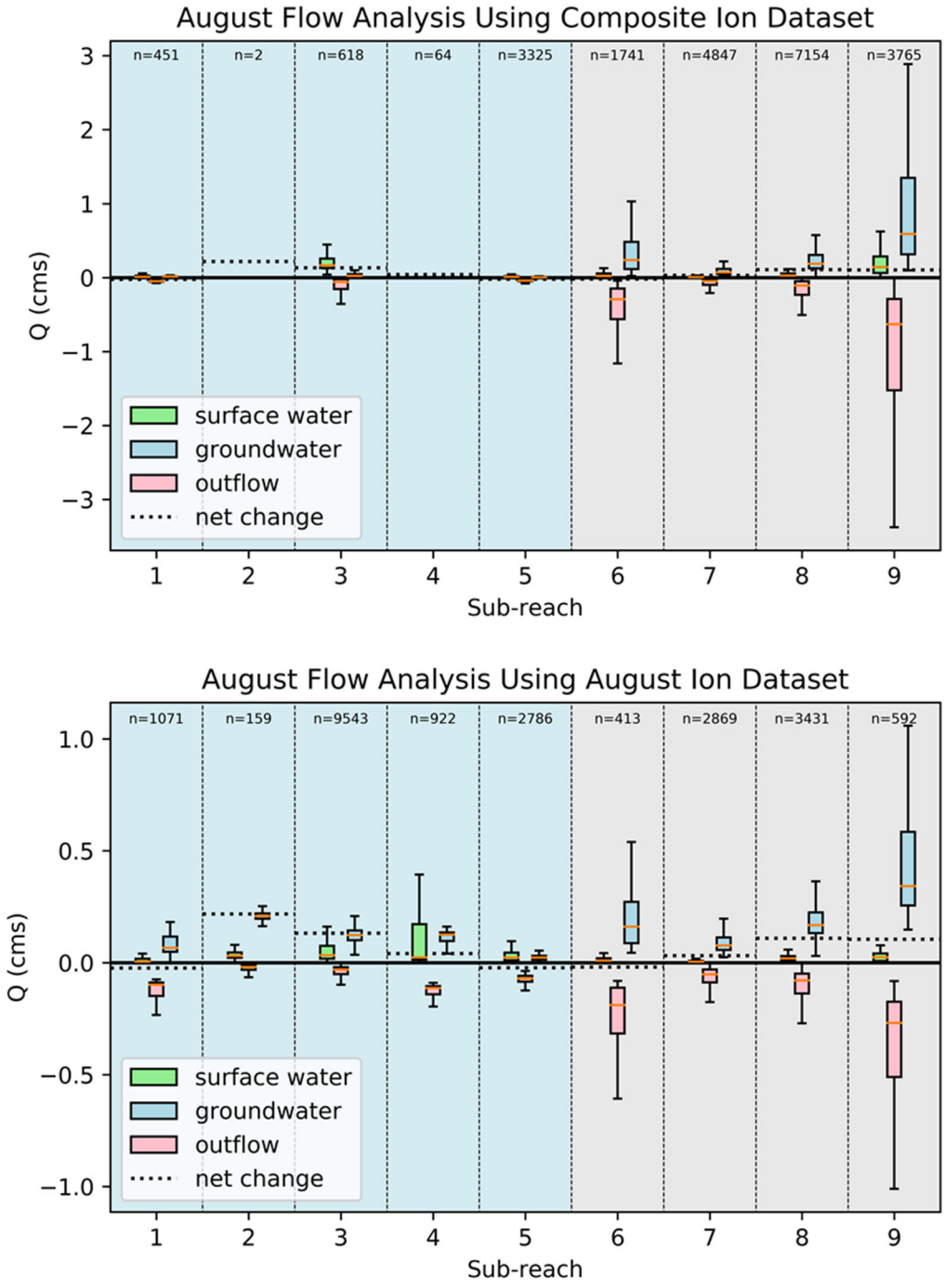

Figure A12. Results of the flow and mass balance analysis for the August 2015 sampling event for reaches with significant flow (i.e., 1st-quartile of a range had a magnitude greater than 5%). If a sub-reach had insufficient solutions (i.e., less than 100 solutions) for Q_{gw}, Q_{sw}, and Q_{out}, boxplots are not shown. The dotted lines represent the ΔQ in each sub-reach.

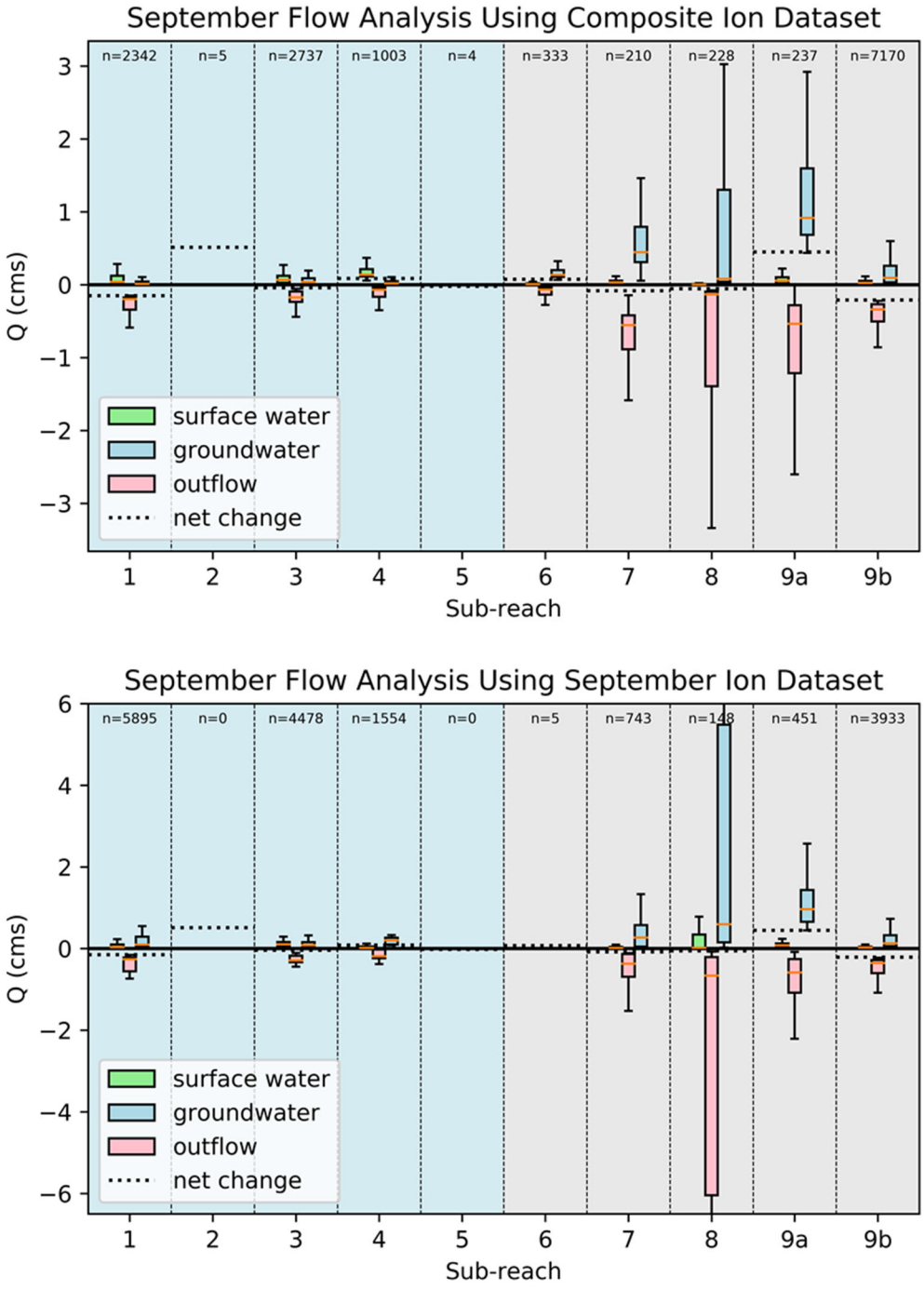

Figure A13. Results of the flow and mass balance analysis for the September 2019 sampling event for reaches with significant flow (i.e., 1st-quartile of a range had a magnitude greater than 5%). If a sub-reach had insufficient solutions (i.e., less than 100 solutions) for Q_{gw}, Q_{sw}, and Q_{out}, boxplots are not shown. The dotted lines represent the ΔQ in each sub-reach.